

12-2011

UNDERSTANDING NANOG'S ROLE IN CANCER BIOLOGY

Mark D. Badeaux

Follow this and additional works at: https://digitalcommons.library.tmc.edu/utgsbs_dissertations



Part of the [Medicine and Health Sciences Commons](#)

Recommended Citation

Badeaux, Mark D., "UNDERSTANDING NANOG'S ROLE IN CANCER BIOLOGY" (2011). *The University of Texas MD Anderson Cancer Center UTHealth Graduate School of Biomedical Sciences Dissertations and Theses (Open Access)*. 205.

https://digitalcommons.library.tmc.edu/utgsbs_dissertations/205

This Dissertation (PhD) is brought to you for free and open access by the The University of Texas MD Anderson Cancer Center UTHealth Graduate School of Biomedical Sciences at DigitalCommons@TMC. It has been accepted for inclusion in The University of Texas MD Anderson Cancer Center UTHealth Graduate School of Biomedical Sciences Dissertations and Theses (Open Access) by an authorized administrator of DigitalCommons@TMC. For more information, please contact digitalcommons@library.tmc.edu.

UNDERSTANDING NANOG'S ROLE IN CANCER BIOLOGY

By

Mark D. Badeaux, B.S.

Approved:

Dean Tang, PhD

Shawn Bratton, PhD

Susan Fischer, PhD

Gary Johanning, PhD

Michael Macleod, PhD

Mark Bedford, PhD

APPROVED:

Dean, The University of Texas
Graduate School of Biomedical Sciences at Houston

UNDERSTANDING NANOG'S ROLE IN CANCER BIOLOGY

A

DISSERTATION

Presented to the Faculty of
The University of Texas
Health Science Center at Houston
and
The University of Texas
M.D. Anderson Cancer Center
Graduate School of Biomedical Sciences
in Partial Fulfillment

of the Requirements

for the Degree of

DOCTOR OF PHILOSOPHY

by

Mark Daniel Badeaux B.S.
Houston, Texas

December 2011

Dedication/Acknowledgements

My scientific career thus far has been an undertaking far more arduous than I had envisioned six years ago as a somewhat callow youth. I thank God for giving me the strength to persevere through numerous perils, scientific and otherwise; for giving me the courage to challenge both my own work and that of others, and for the perspective to follow my moral compass in truly understanding what's important in life. I am blessed to have been raised by two wonderful parents, one of whom I lost to colon cancer 12 years ago and from whom I constantly draw strength. My foray into research science also brought an amazing woman into my life, and I can honestly say that without Aimee I would be incomplete and a lesser person. Having her support has made this journey much easier, and loving her gives me strength when I feel as if I am bereft of it. I am especially indebted to my Shame dog, who gave me unconditional love for all of his 16 years, who made me laugh every day, and whose unflagging optimism made it impossible to be weighed down by the burdens of life and science. A special thanks to my siblings (my brother, Chris and my sisters, Adri and tha B) as well-they give me both perspective and hope, and always a dose of reality when needed.

I would like to thank my mentor Dean Tang- truly, I was not a scientist nor did I know what it meant to be one when I arrived on campus, but have learned to be a good one in no small part because of his constant cajoling, teaching, demanding, and inspiring. The Tang Lab also deserves thanks for both their friendship and their help everyday in tackling the great unknown. I would like to single out Jichao Qin for praise here, for he truly is my favorite (we're not supposed to have favorites?) of all who have

called themselves Tang Lab members. I miss his humor, I admire his work ethic, and I will never forget when he inadvertently told Aimee that I was going to propose to her *before* I had proposed to her.

A number of individuals deserve acknowledgement for their contribution to this work. Among these I include each member of my Supervisory committee, as well as Bigang Liu, Joyce Rundhaug, and Donna Kusewitt for the pearls of wisdom and practical help they offered me along the way.

I would like to finish by simply thanking Science Park, for I cannot list everyone who has helped me with either a smile or a protocol (or both), but suffice it to say that Science Park has left an indelible mark on me, one which I hope to carry with me in my scientific career as a badge to be displayed proudly.

UNDERSTANDING NANOG'S ROLE IN CANCER BIOLOGY

Mark Daniel Badeaux, B.S.

Supervisory Professor Dean Tang, PhD

The cancer stem cell model holds that tumor heterogeneity and population-level immortality are driven by a subset of cells within the tumor, termed cancer stem cells. Like embryonic or somatic stem cells, cancer stem cells are believed to possess self-renewal capacity and the ability to give rise to a multitude of varieties of daughter cell. Because of cancer's implied connections to authentic stem cells, we screened a variety of prostate cancer cell lines and primary tumors in order to determine if any notable 'stemness' genes were expressed in malignant growths. We found a promising lead in Nanog, a central figure in maintaining embryonic stem cell pluripotency, and through a variety of experiments in which we diminished Nanog expression, found that it may play a significant role in prostate cancer development. We then created a transgenic mouse model in which we targeted Nanog expression to keratin 14-expressing in order to assess its potential contribution to tumorigenesis. We found a variety of developmental abnormalities and altered differentiation patterns in our model, but much to our chagrin we observed neither spontaneous tumor formation nor premalignant changes in these mice, but instead surprisingly found that high levels of Nanog expression inhibited tumor formation in a two-stage skin carcinogenesis model. We also noted a depletion of skin stem cell populations, which underlies the wound-healing defect our mice harbor as well. Gene expression analysis shows a reduction in c-Jun and Bmp5, two genes whose loss inhibits skin tumor development and reduces stem cell counts respectively.

As we further explored Nanog's activity in prostate cancer, it became apparent that the protein oftentimes was not expressed. Emboldened by the competing endogenous RNA (ceRNA) hypothesis, we identified the Nanog 3'UTR as a regulator of the tumor suppressive microRNA 128a (miR-128a), which includes known oncogenes such as Bmi1 among its authentic targets. Future work will necessarily involve discerning instances in which Nanog mRNA is the biologically relevant molecule, as well as identifying additional mRNA species which may serve solely as a molecular sink for miR-128a.

Table of Contents

I. K14.Nanog transgenic mouse model

Chapter 1- Introduction and Background	1
Adult stem cells and the cancer stem cell model	1
Embryonic stem cells and cancer	4
Nanog in ES cells	6
Nanog in cancer	8
Mouse skin and skin stem cells	10
Two-stage skin carcinogenesis	14
Anatomy of the prostate	17
Proliferative diseases of the prostate	18
Chapter 2- Materials and Methods	20
Chapter 3- Characterization of K14.Nanog Mice	28
Dose-dependent phenotypes in K14.Nanog mice	30
Phenotypes-skin	31
Wound healing defect in K14.Nanog mice	33
Phenotypes-lens	38
Phenotypes-lingual/digestive	39
Phenotypes-thymus	40
Chapter 4- Testing Nanog's Effect on Tumor Development	44
Lack of tumor development in transgenic mice	44
Chapter 5- Skin Stem Cells and Gene Expression Analysis	50

Assessment of skin stem cell populations	50
Chapter 6- Ongoing and Future Studies, Significance	58
Prostate-specific Nanog expression: A constitutive model	58
Summary/Significance	59
Future Studies	60
 II. Nanog and miR-128a	
Chapter 7-Introduction and Background	63
MicroRNA- general information	63
MicroRNAs and non-coding RNA species	66
MicroRNA 128a- a candidate tumor suppressor	67
Chapter 8- Materials and Methods	70
Chapter 9- Examining the Nanog/miR-128a Axis	73
Nanog regulation by miR-128a	70
Mir-128a as a tumor suppressor in PCa	73
Nanog mRNA miR-ly as a sponge?	75
Chapter 10- Significance and Future Directions	78
<i>References</i>	83
<i>Vita</i>	98

List of Illustrations

I. K14.Nanog transgenic mouse model

Figure 1-1 The Nanog protein	9
Figure 1-2 Stem cell populations in the murine hair follicle	15
Figure 3-1 Characterization of K14.Nanog transgenic mice	34
Figure 3-2 Nanog protein expression in transgenic mice	35
Figure 3-3 Characterization of Line 1 skin abnormalities	36
Figure 3-4 K14 Nanog mice exhibit a wound-healing defect	37
Figure 3-5 Shared lens phenotype between transgenic mice	41
Figure 3-6 Digestive and Thymic Phenotypes at P5	42
Figure 3-7 Abnormal differentiation K14. Nanog tongue	43
Figure 4-1 Two-stage skin carcinogenesis	48
Figure 4-2 Hyperplastic response to TPA treatment	49
Figure 5-1 Diminution of hair follicle stem cell pools	51
Figure 5-2 Epidermal gene expression panel	56
Figure 5-3 c-Jun levels are reduced in K14.Nanog epidermis	57
Figure 6-1 Characterization of ARR ₂ Pb Nanog Mice	62

II. Nanog and miR-128a

Figure 9-1 Mir-128a can regulate the Nanog 3'UTR	76
Figure 9-2 Lowering Nanog levels increases miR-128a levels	77
Figure 9-3 Mir-128a lessens PCa clonal and clonogenic growth	78

List of Tables

I. K14.Nanog transgenic mouse model

Table 3-1 Summary of BK5.Nanog injections	29
Table 4-1 K14.Nanog/K5.Myc breedings	45
Table 5-1 Primers used in epidermal gene expression studies	55

I. K14. Nanog Transgenic Mouse Model

Chapter 1- Introduction and Background

Introduction

Tumors are immortal, heterogeneous tapestries woven of various malignant cells, yet these disparate threads do not all have the same malignant potential. The cancer stem cell model posits a hierarchy existing in tumor cells that is similar to hierarchies that may be found in many adult somatic tissues. In an effort to understand at the molecular level some of the resemblance between cancer cells and stem cells, we have identified a number of stem cell genes that are expressed in prostate cancer and have focused on a particularly interesting master regulator of embryonic stem cells known as Nanog. Extensive loss-of-function studies demonstrated that Nanog depletion greatly inhibited tumor development in xenograft models of prostate cancer. In order to model a potential role for Nanog in tumorigenesis, we created transgenic mice in which tumor-derived Nanog cDNA is driven by the keratin 14 promoter, thereby targeting its expression to a variety of stem cell populations.

Background

Adult stem cells and the cancer stem cell model

For many years it has been appreciated that tumors are possessed of multifarious cell types; what is less clear is the origin of these disparate sorts of cell. Long-standing dogma has it that genetic instability in tumor cells produces competing cells within a tumor; cells that bear mutations that confer a selective advantage become dominant (1). This clonal evolution model is thought to operate dynamically and constantly in cancer,

such that sharp changes in the tumor's environment (such as those that occur when chemotherapy is begun) are met with an ever-adapting population. In sharp contrast to this model is the cancer stem cell (CSC) hypothesis, which postulates that cells bearing many of the same properties as adult stem cells generate the myriad cell types present in a given tumor (2); these properties may include self-renewal, relative dormancy, and an increased tolerance for genomic damage (as often occurs in chemotherapeutic regimens).

In normally-functioning adult organs, tissues are highly organized and, for the most part, are arranged in a discernibly hierarchical manner with stem cells occupying the apex. Oftentimes, the immediate progeny of adult stem cells is the transit-amplifying (TA) cell, also known as the progenitor cell. These cells are characterized by high immediate proliferative activity, and the progenitor sits upstream of mature, terminally-differentiated cells. This latter cell type is the functional effector of its respective organ, and is characterized by a highly-specialized transcriptional program. These cells have also irrevocably committed to their fate, and are generally believed to lose the ability to proliferate. The notion that similar hierarchies exist in cancers is not a new one, but with the emergence and refinement of several techniques, especially fluorescence-activated cell sorting (FACS), amenable to isolating cell populations of interest, this notion has been much easier to test. The CSC model gained significant traction in the mid-1990's after two seminal studies by the Dick lab involving acute myelogenous leukemia (AML) in which they demonstrated that CD34⁺, CD38⁻ cells alone could generate transplantable leukemia (3, 4). CD34⁺/CD38⁻ is, not coincidentally, the cell-surface phenotype borne by human hematopoietic stem cells.

There has been much confusion in the scientific community due to the moniker “cancer stem cell”. The term is functional and refers to the cell population that can regenerate tumors in a xenograft setting; to demonstrate self-renewal (of the tumor) with a reasonable degree of certainty, xenografts are done iteratively for several generations of tumor. Additionally, these tumors must recapitulate the heterogeneity seen in the parental tumor to fully fit the definition of cancer stem cell. This heterogeneity is thus assumed to arise from the ability of the CSC to give rise to its own spectrum of cancerous progeny. CSCs need not necessarily originate from normal stem cells, although it is quite likely that, owing to the long-lived nature of adult stem cell populations, these more primitive cells are indeed prime targets for transformation. Progenitor cells, having replicative ability and some limited self-renewal abilities, may also suffer genetic and epigenetic alterations that yield CSCs. It is unknown if terminally differentiated cells can undergo dedifferentiation or can be transformed into cancer stem cells, although such a scenario is considered unlikely.

Also unknown is whether solid tumors are arranged hierarchically, as many blood cancers seem to be. One of the earliest reports identified cancer stem cells in breast cancers (5), although the fact that the samples utilized were not primary tumors, but rather pleural effusions and metastases, left open the question of whether or not primary breast tumors in fact were arranged in a hierarchy. In the past ~7-8 years, there has been a deluge of reports claiming identification of CSC populations in nearly every sort of solid tumor. Upon closer inspection, however, many of these reports are incomplete, oftentimes lacking the gold standard of serial *in vivo* xenotransplantation assays and/or demonstration of phenotypic heterogeneity in tumor regrowths.

The question of whether prostate cancers behave according to the cancer stem cell model is the subject of many labs' research, including our own. This question has been impossible to definitively address, as technical limitations render xenograft regrowth of primary prostate tumors null. This is even true when employing different sites of injection and/or adding Matrigel or other reagents to augment cell engraftment. Instead, xenograft prostate tumors or tumors derived from pre-established cancer cell lines, e.g., PC3, DU145, and LNCaP have been used as surrogates in these experiments. In this context, it has been shown that CD44⁺ cells are significantly enriched in CSC activity (6).

Embryonic stem cells and cancer

Superficially, one may see a resemblance between an embryo and a cancerous growth, in that both have a high rate of proliferation, near-limitless proliferative potential, and exist in an undifferentiated state. However, the embryo is carrying out a highly orchestrated program that results in a functional organism, whereas the neoplasia grows wantonly. There remains nonetheless a connection between the two, for the embryo and its *in vitro* derivative, the embryonic stem cell (ES cell), possess two traits important for sustained activity: They are multipotent, that is, they can give rise to numerous cellular lineages, and they possess the quality of self-renewal, or the ability to replenish themselves at the population level. Both of these qualities are evident in cancers as well, leading one to wonder if perhaps they share any common molecular features as well. In the past four years, a number of groups have conducted large-scale gene expression forays in which similarities between ES cells and various cancers,

including lung and bladder malignancies, have been noted (7-9). An underlying assumption of such similarities is a global similarity in epigenetic landscape that is then manifested in the form of gene expression mimicry. It has been reported that intractable hypermethylation of the promoter regions of Polycomb group target genes occurs both in ES cells and in many cancer cells as well (10); enticingly, many of these genes are established or candidate tumor suppressors. Additionally, it has been speculated that the presence of a bivalent chromatin state in ES and adult stem cells, one composed of methylation at the tail of histone 3 at lysine 27 and at lysine 4, and one that is believed to be poised for activation of neighboring genes, may predispose cancer cells to repression of these genes through a scant few additional repressive events (11).

Reports of shared gene expression such as those enumerated above raised the question as to whether or not ES cells share common transcriptional machinery with somatic cancer cells. Nanog, Oct4, and Sox 2 represent the core triad of transcription factors that serve to maintain the pluripotent (able to give rise to all cell lineages save placental) state, acting as hubs in a large-scale protein network dedicated to pluripotency (12, 13). Quite often, these transcription factors work together, occupying each other's promoters and binding many common promoter regions as well (14). In fact, binding of multiple (more than four) transcription factors is oftentimes required for gene expression from a particular locus in ES cells, and those genes with low transcription factor occupancy tend to be inactive (13).

Numerous studies have claimed re-expression of ES cell transcription factors in human cancers, although closer inspection reveals that the most substantive data is found at the level of mRNA expression, while confirmed reports of the ES cell transcription

factors themselves, such as Nanog's role in glioma stem cells (15), are scarce. There have been, however, a number of systems generated in order to test the *potential* contribution of these molecules to cancer development, e.g., Oct-4 and Nanog, when expressed together in a lung adenocarcinoma cell line (A549), result in increased *in vitro* sphere formation, an increase in the putative CSC population marked by CD133+, and larger tumors in a subcutaneous xenograft assay of tumor development (16). The most compelling of these systems has been in the form of transgenic mouse models; because transcription factors are likely to exert highly cell-type-specific effects (see Klf4, whose overexpression in the breast is tumor inhibitory but leads to dysplasia in epidermal basal keratinocytes (17-19)), systems that target multiple organs are likely to yield the most comprehensive and useful insights. A provocative study performed by the Jaenisch lab, which employed a doxycycline-inducible mouse model of Oct-4 overexpression from the *Collagen1a1* locus, demonstrated epithelial dysplasia and epidermal tumor growth upon activation of Oct-4 (20). The authors concluded, however, that despite its powerful *potential* contribution to tumor development, it was surprising that the molecule was rarely re-expressed in human tumors. This fact suggested to them that the molecule was under epigenetic "lock and key," perhaps because of its oncogenic potential.

Nanog in ES cells

As mentioned previously, Nanog is a homeobox transcription factor essential to maintaining pluripotency; it consists of 305 amino acids in both human and mouse homologues, and as such has a predicted molecular mass of 34 kilodaltons (Figure 1-1). The human and mouse Nanog proteins are ~60% similar at the amino acid level, but the

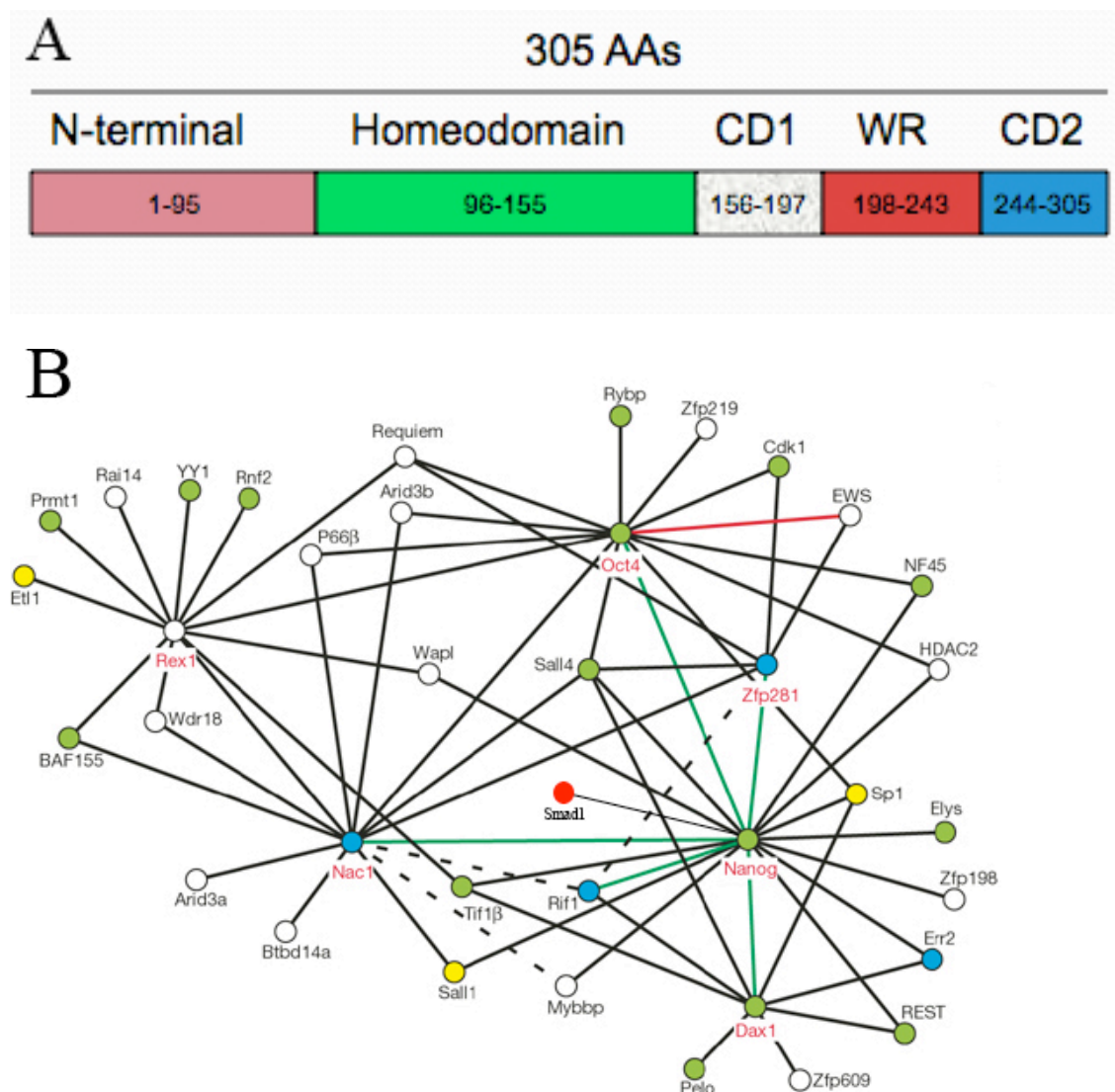
critical DNA-binding domains of the two proteins share over 90% homology. The protein is organized into five functional domains: The N-terminal domain seems to represent a docking site for other proteins (21), while the homeodomain is responsible for DNA-binding. The C-terminal domains have transactivating ability (22-24), and between them lies the unique tryptophan repeat domain in which every fifth amino acid residue is a tryptophan. This WR region is essential for Nanog dimerization, without which it cannot function to propagate the pluripotent state (25). In ES cells, Nanog exists in a variety of protein complexes that range in size from 160kD to over 1 megadalton (12). Its gene was cloned as part of a cDNA library screen to identify factors responsible for scant yet reproducible mouse ES cell propagation in the absence of leukemia-inhibitory factor (LIF) (26, 27), which is necessary for mouse ES cell growth but dispensable for proliferation of human ES cells. ES cells that have been engineered to lack Nanog can surprisingly self-renew, but in chimeric mice these cells cannot form functional germ cells. Due to its role in establishing the inner cell mass (ICM) of embryos as well as in creating mature germ cells, it has been postulated that Nanog serves to resist differentiation signals, holding open a figurative window of pluripotency (28).

The vast body of scientific study that has arisen in the wake of Yamanaka and colleagues' discovery that adult somatic cells can be reprogrammed into ES-like cells called induced pluripotent cells (iPS cells) (29) has also led to insights concerning the factors that are crucial for this process. Unsurprisingly, Nanog is a central figure in this reprogramming: Without Nanog, partially de-differentiated/reprogrammed intermediates cannot attain full pluripotency. ES cells that lack Nanog cannot invoke

reprogramming of somatic cells in the context of cell fusion, and Nanog has also been found to mark the developing epiblast. In fact, in the absence of Nanog, the ICM forms but cannot attain full pluripotency; for this and the reasons enumerated above, it has been suggested that Nanog acts as the conduit to “ground state pluripotency” (30).

Nanog in cancer

Nanog expression has been reported in a variety of cancer types at the protein level, e.g., (31-33), although the veracity of many of these reports is questionable due to several concerns including reagent specificity. More compelling evidence of Nanog gene expression exists in the form of mRNA-related data, e.g., (34-37). Our lab conducted pilot studies in a variety of prostate cancer cell lines, xenografts, and primary tumors in order to determine which potential stem cell factors were expressed in this spectrum of diseases, and found consistent expression of a Nanog retrogene, NanogP8, which encodes a protein identical to that encoded by the canonical *Nanog* gene (38). We then asked whether expression of Nanog may be important in tumor development. To answer this question, we conducted loss-of-function studies, utilizing Nanog small interfering RNA (siRNA) to show that diminishing Nanog levels reduces *in vitro* serial sphere-propagating ability, and utilizing lentiviral-mediated short hairpin RNA (shRNA) to show decreased tumorigenesis in subcutaneous xenografts of various cancer cell lines. For technical reasons, including unexplained cell death when overexpressing Nanog cDNA, we decided to conduct gain-of-function studies in a transgenic mouse model.

Figure 1-1**Figure 1-1 The Nanog protein**

Nanog is a transcription factor comprised of 305 amino acids which has five known functional domains, as depicted in (A). It is one of the central hubs in the protein-protein interaction network devoted to maintaining pluripotency in the ICM(B), and associates cooperatively with other hub molecules such as Oct4, or repressively as exemplified by its binding to Smad1 which blocks Bmp signaling.

Figure 1-1B is adapted from Wang *et al.* 2006 Nature 444:364-368.

We chose to utilize the keratin 5/keratin 14 promoters as they target basal cell populations in stratified squamous epithelia (39-42); these basal cells are known to harbor stem and/or progenitor cell populations. These promoters have been shown to cause the most dramatic phenotypes in the skin, as promoter expression is strongest in this tissue. Additionally, we chose to target the prostate, as most of our Nanog studies centered on prostate cancer, and therefore utilized the ARR₂Pb promoter which has activity primarily in luminal cells of the prostate (43, 44).

Mouse skin and skin stem cells

The skin is a protective organ whose primary role is to serve as a barrier between an organism and its environment, and it is composed of three important regions: The **epidermis** is home to epithelial cells that are nucleated, express keratins 5 and 14 (K5 and K14), and are situated near the basement membrane but enucleate as they detach, begin to express keratins 1 and 10 (K1 and K10), and move suprabasally to form the highly keratinized, waxy outer layer of skin. The **dermis** is populated chiefly by fibroblasts and is the region in which hair follicles and sebaceous glands are anchored. The **hypodermis** is primarily composed of fat and is an important mediator of temperature regulation, one of the skin's ancillary duties. Contributing to this phenomenon in humans are sweat glands that secrete fluid when body temperature rises; evaporation of sweat removes heat from the body. In colder climes, body hair serves to retain heat. Mice lack the ability to sweat but retain body heat in part through the copious amount of fur that covers most of the animal, save the tail and feet.

Anatomically, this distinction means that hair follicular density in mouse skin is much greater than that in human skin.

The differences in anatomical structure between adult human and mouse skin extend to the location of their respective stem cell populations. In human skin, the basal layer of the epidermis has been shown to harbor cells capable of extensive clonal growth *ex vivo*. Because of the relative paucity of hair follicles in the human skin, it is thought that the basal epidermal keratinocytes are the primary stem cell pool. It should be noted that many of the techniques available to study mouse skin, such as lineage tracing and label-retention, are quite obviously not available to employ in human systems for ethical reasons, and therefore knowledge of human skin stem cells is scant when compared with the findings in mouse skin.

The murine interfollicular epidermis (IFE) is home to a population of basal cells with capacity for clonal expansion *in vivo* during steady-state conditions, and is thought to be the hub of the so-called epidermal proliferative unit (EPU) coined by Chris Potten (45). There is some controversy as to whether these cells represent true stem cells or so-called progenitor/transit-amplifying cells, but this may be a semantic argument, as functionally these “stem” cells are responsible for clonal repopulation of a localized area of the IFE.

Adult mouse skin’s resident stem cells are primarily localized in the hair follicle, and consist of several distinct populations, although it should be noted with some caution that the degree of overlap as well as the lineage relationships among these populations has not been fully explored, and given the rash of new stem cell populations

discovered in this tissue in the past two years, it is likely that there are as-yet-undiscovered mouse skin stem cells.

The classical method for identifying mouse skin stem cells is the label-retaining experiment, first conducted using tritium-laden thymidine that is incorporated into DNA during S phase of the cell cycle (46), and now commonly performed using 5'-bromo 2'-deoxyuridine (BrdU) in its stead. Label-retaining cells (LRCs) are identified by first pulsing the mouse with the label to be used; the pulse is performed for a sufficient length of time such that all cells under study have been allowed to proliferate, and therefore have taken up the label. The subsequent "chase" period is the empirically-determined window of time that the label is diluted through multiple rounds of cell division; only cells that have remained relatively quiescent during the chase will still bear the initial label at a detectable level. This method for detecting quiescent skin cell populations revealed the presence of LRCs in the bulge region of the hair follicle as well as in the basal layer of the IFE.

Ex vivo, keratinocytes (usually from newborn mice, although adult keratinocytes can be used as well, albeit at much lower efficiencies) can be plated at clonal density on a low (~one-third confluent) density of 3T3 mouse fibroblast cells or on a variety of substrates (e.g. laminin, collagen IV) in defined media supplemented with growth factors and allowed to form colonies. Tightly packed growths, known as holoclones, are believed to contain stem cells, whereas less-organized meroclones and paraclones may contain progenitors and differentiated cells, respectively (47).

The preferred current method of distinction among various cell populations is by way of cell-surface marker profile, since these populations can be prospectively isolated

by FACS and assayed for stem cell function by engrafting the population of interest, along with newborn dermal fibroblasts, onto the backs of immunocompromised mice and assessing the degree of contribution to new IFE, hair follicles, and sebaceous glands.

The chief resident hair follicle stem cell population is thought to be the α -6 integrin⁺, CD34⁺ cells in the bulge region. A subset of these cells additionally are LRCs, and this population is capable of reconstituting the epidermal lineages, including the IFE, the hair follicle, and the sebaceous gland, in their entirety. Current thought therefore places these cells at the top of the hair follicle stem cell hierarchy, as they demonstrate multipotency *in vivo* and in *ex vivo* artificial systems.

Bulge cells co-expressing CD34 and leucine-rich repeat-containing G-protein-coupled receptor 5 (Lgr5) surprised researchers as they were found to be able to reconstitute all epidermal lineages in transplantation experiments but were also found to be actively cycling (48). This finding challenged the paradigm of stem cells in the skin existing solely in a relatively quiescent state.

The observation that upon wounding, stem cells are surprisingly recruited from the infundibulum and isthmus rather than from the bulge and contribute significantly to the repair of affected areas, suggests that bulge keratinocytes are not the only reservoir of follicular stem cells. Leucine-rich immunoglobulin-like 1 (Lrig1)-positive cells lie in the junctional zone between the infundibulum and the IFE. As Lrig1 is a transmembrane, cell surface protein whose known role is to restrict epidermal growth factor receptor (EGFR) signaling by targeting it for ubiquitination and therefore degradation following EGFR stimulation (49, 50), it is thought to promote a relatively quiescent state. Although Lrig1⁺ cells are capable, when mixed with neonatal dermal

fibroblasts and grafted onto immunocompromised hosts, of reconstituting all epidermal cell types, lineage tracing experiments suggest that this population replenishes only the IFE and the sebaceous glands during normal homeostasis (51).

Leucine-rich repeat-containing G-protein-coupled receptor 6 (Lgr6)-positive cells represent an interesting population, as they generate the three epidermal components prenatally, yet the adult population directly above the bulge only gives rise to IFE and sebaceous gland, but was found to be involved in wound repair (52). There is some overlap between the Lrig1⁺ and Lgr6⁺ populations, but the extent of this shared pool has not been analyzed.

MTS 24-positive cells consist of two sorts: Some lie directly above those cells that express CD34, and it has been noted that this population contains LRCs, although its ability to reconstitute hair follicles in a transplantation assay is unknown (53). Another population cycles actively and has been shown to generate the three broad epidermal cell types .

Two-stage skin carcinogenesis

A two-stage chemically-induced carcinogenesis protocol is among several experimental models available to researchers with an interest in studying tumor development in the skin. It lists among its strengths the ability to delineate between the initiation and promotion phases of tumor development, and is easily superimposed upon pre-existing transgenic or knockout mouse lines as both the initiator and promoter may be delivered topically.

Figure 1-2

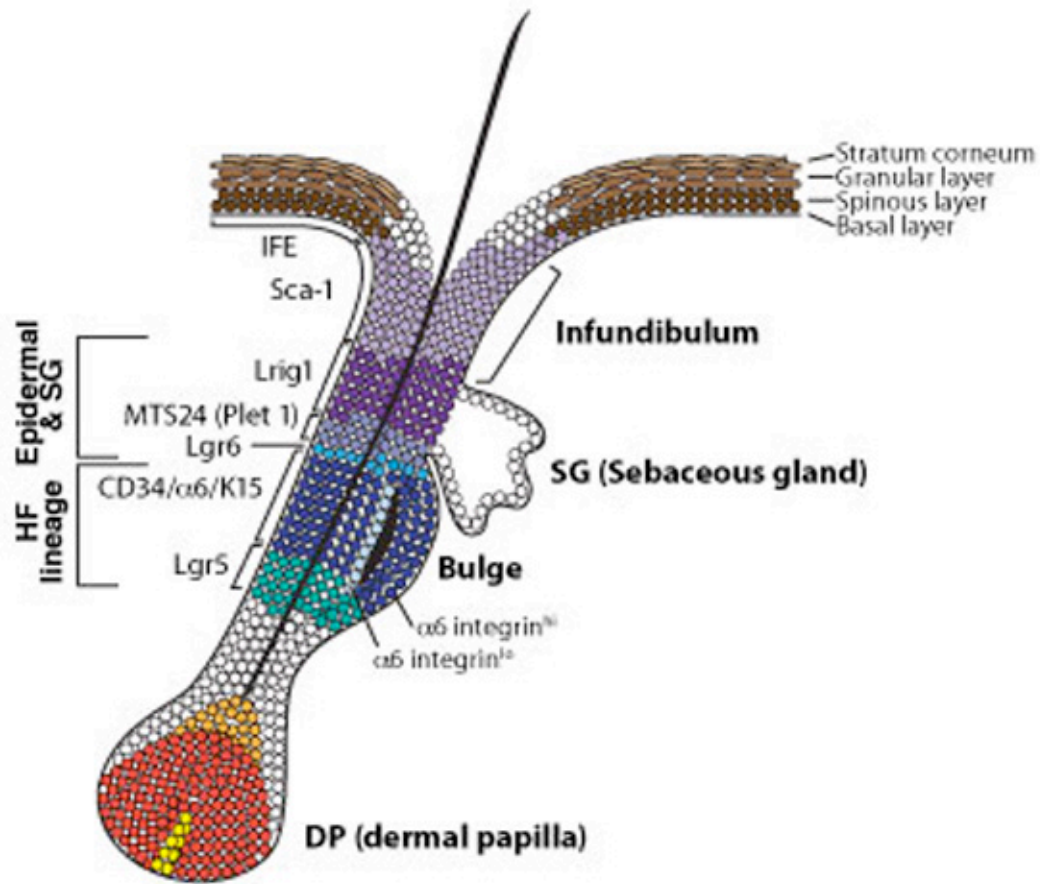


Figure 1-2 Known stem cell populations in the murine hair follicle

A number of cell-surface markers define stem cell populations in the hair follicle. The degree of overlap and lineage relationship among the various populations is currently the subject of much research. For further descriptions of each stem cell population please see the body of the text.

Genetic lesions are introduced into skin stem and progenitor cells (54) found in both the interfollicular epidermis and the hair follicle (55) by application of a single sub-carcinogenic dose one of a diverse array of initiating compounds, among which 7,12-dimethylbenz[a]anthracene (DMBA) is the most widely used. Two members of the *Ras* G protein-coupled receptor family, *Hras* and *Kras*, sustain the relevant DMBA-induced mutational burden, resulting in largely dormant mutation-bearing cell populations that await proliferative stimuli in order to clonally expand. It should be noted that the genetic insults induced by many initiators, including DMBA, are largely irreversible; accordingly, intervals between initiator and promoter treatment may span a range from two weeks to many months.

After the initiator has been allowed sufficient time to be metabolized, the tumor promotion phase may begin. Typically, 12-O-Tetradecanoylphorbol-13-acetate (TPA) or another phorbol ester compound is used to induce cellular proliferation. TPA does so by activating Protein Kinase C (PKC), as TPA resembles diacylglycerol, one of PKC's endogenous triggers. PKC phosphorylates many proteins at serine and threonine residues; among the most important in the context of its activation in the two-stage carcinogenesis protocol is epidermal growth factor receptor (EGFR). Indeed, signaling through PKC and in turn through EGFR has been shown to also activate Akt (protein kinase B) as a further downstream consequence (56). Essentially, a host of phosphorylation events are initiated and signaling pathways activated when TPA is applied to the skin. The tumor promoter is generally applied topically two or more times per week, and it is essential that a regular schedule is adhered to, as the effects of

promoters are reversible, i.e., hyperplasia or papillomas induced by promotion will recede in the absence of treatment. Promotion may last for 20 weeks to a full year, and during this time course epidermal hyperplasia will yield benign exophytic papillomas; cells in these small tumors may eventually sustain sufficient additional genetic insults such that the papilloma will progress to a squamous cell carcinoma (SCC). SCCs resulting from the two-stage skin carcinogenesis protocol are in many respects similar to those that occur spontaneously in humans, and may be identified by their endophytic, vascularized nature.

There are several practical advantages to using a two-stage protocol rather than a one-stage, or complete, method. In the latter, the distinction between initiation and promotion is obfuscated, while in the former both are readily separable (57). In such a setting, a gene or compound of interest may be more accurately described with respect to its role in skin carcinogenesis. Additionally, a gene's contribution to the progression from premalignant lesion to frank cancer may also be assessed. In any skin carcinogenesis protocol, mouse models that are recalcitrant to spontaneous tumor development may still be studied in the context of carcinogenesis.

It is also important to note the limitations of this experimental model. First, it does not accurately recapitulate the genetic underpinnings of human skin cancer, as SCCs in this model are Ras-driven, while human skin cancers are largely reliant on p53 inactivation (58). Additionally, it cannot be used to address other cancer types due to the need for topical application of the relevant chemicals. Finally, metastasis of the SCCs produced is rare, relegating the protocol chiefly to the study of benign growths and primary tumors.

Anatomy of the prostate

The prostate is a small, hormone-responsive, exocrine organ tasked with producing and secreting fluids that aid in sexual reproduction. The mouse prostate is grossly unlike that of humans, in that the latter is a small uniform walnut-sized organ while the former contains four lobes (anterior, dorsal, lateral, and ventral) arranged around the urethra. Histologically, however, the two are organized similarly: The tubules that comprise the gland possess epithelial cells that overlie supporting stroma. The prostatic epithelium consists of basal cells that are anchored to the basement membrane and that express K5 and K14, differentiated secretory luminal cells that express keratins 8 and 18 (K8 and K18), and neuroendocrine cells that are interspersed throughout the basal layer.

The most commonly used construct for targeting a gene of interest to the prostate is the androgen-responsive probasin promoter, or more properly, the artificial derivative known as the ARR₂Pb promoter, which has two androgen response regions (ARRs) immediately upstream of the minimal probasin promoter (44). Genes cloned into constructs bearing this promoter are expressed primarily in the luminal cells of the mouse prostate, although scant expression in basal and even stromal compartments can be observed (unpublished observations). Expression is likewise stronger in some lobes than others, with dorsal and ventral expression being much higher than expression in the anterior prostate ((44) and unpublished observations). The promoter is extremely sensitive to androgen levels, and as such achieves maximum activity as the mouse reaches sexual maturity at roughly eight weeks of age (44).

Proliferative diseases of the prostate

Two of the most common diseases of the prostate are benign prostatic hyperplasia and prostate cancer. The latter is of particular importance since it may metastasize and cause significant mortality in untreated or treatment-refractory male populations. Prostate cancer in humans occurs in a multi-step fashion, from normal gland to prostatic intraepithelial neoplasia (PIN) lesion to prostatic adenocarcinoma. The cell of origin for prostate cancer is a point of contention among various groups, but decades of pathological evidence suggests that luminal expansion is the primary manifestation of the disease.

Chapter 2- Materials and Methods

Mouse Housing and Care

All housing and procedures were carried out in an animal facility accredited by the American Association for the Assessment and Accreditation of Laboratory Animal Care, in accordance with Institutional Animal Care and Use Committee guidelines. Mice were fed *ad libitum* unless otherwise noted.

Generation of K14-NanogP8 Mice

The basic procedures for establishing transgenic (Tg) animals have been previously described. Briefly, the NanogP8 open-reading frame cDNA derived from HPCa5T, a primary human prostate tumor, was cloned into the multiple cloning site (MCS) of the pBluescript-human keratin 14 vector, in which the human keratin 14 promoter is immediately followed by a rabbit b-globin intron and the MCS is followed by an SV40 poly-A tail (see Fig. 1-1A for a schematic). The K14 promoter directs expression to several tissue types, including basal cells of the skin, prostate, bladder, forestomach, tongue, mammary myoepithelium, kidney papilla, and pancreatic ductal epithelia.

Screening for K14-Nanog Mice

Mouse tail snips or ear punches were collected and lysed in a solution containing 25 mM NaOH and 0.2 mM EDTA at 95°C for 30 minutes, after which neutralization buffer (40 mM Tris-HCl, pH 5) was added (HOTSHOT PROTOCOL). Five mL of this sample was added to 20 mL polymerase chain reaction (PCR) reaction mixture

consisting of 12.5 mL 2x GoTaq Mastermix (Promega), 5.5 mL ddH₂O, and 1 mL each of b-globin forward primer (5'-GGG-CAA-CGT-GCT-GGT-TAT-3') and NanogP8 reverse primer (5'-CCT-TTG-GGA-CTG-GTG-GAA-3') at 10 mM. PCR was carried out for 35 cycles consisting of a standard melting step, an annealing temperature of 58°C and a 45-second extension at 72°C. Products were run on a 1.5% agarose gel containing ethidium bromide and were visualized using UV light. Transgenic mice were identified as those bearing a ~300-bp product. Alpha Imager software (Alpha Innotech) was used to collect images.

Epidermal Lysate

Mouse dorsal skin was shaved and Nair was applied to remove remaining hair stubble. The hair-free skin was scraped on ice using a straight-blade razor and epidermis was scraped until shiny dermis was evident. The epidermal scrapings were added to lysis buffer containing 25 ul/mL protease inhibitor cocktail (Sigma) and mixed thoroughly and the mixture was incubated for ~1 h. The lysate was centrifuged at 16,000 g for two minutes at 4°C and the supernatant was used to perform Western blot.

Harvest of Murine Organs

Mice were sacrificed using constant-flow CO₂ followed by cervical dislocation. Internal organs were removed quickly, placed directly into microcentrifuge tubes, and were then immersed in liquid nitrogen (for Western blot). Alternatively, the organs were placed into cassettes, which were immersed in 10% formalin for 24-48 h followed by immersion in 70% ethanol (for immunohistochemistry). Organs were embedded in

paraffin, sectioned, and placed on glass slides. Organ protein lysate was made by cryopulverizing the tissue then immersing the powder in chilled lysis buffer containing 25 mL/mL protease inhibitor cocktail (Sigma). The lysate was centrifuged at 16,000 *g* for two minutes at 4°C and the supernatant was used to perform Western blot.

Western Blotting Analysis

Protein samples were loaded in equal amount in each well of a 12.5% polyacrylamide gel and electrophoresed until the protein ladder was fully resolved. Proteins were then transferred to nitrocellulose membrane (Biorad), which was blocked using 4% milk in TBST (Tris-buffered saline with Tween). Primary antibodies were diluted in 4% milk/TBST and were incubated on the membrane at 4°C overnight, then washed three times with TBST. Appropriate horseradish peroxidase-conjugated secondary antibodies were added at a 1:2000 dilution using 4% milk/TBST as a diluent and incubated for one hour at room temperature. The membrane was washed three times with TBST and luminescence was produced using Western lightning ECL plus detection reagent (Perkins Elmer).

Immunohistochemistry (IHC)

Tissues were embedded in paraffin blocks, and 4- μ m sections were cut. Slides were deparaffinized in xylene or a xylene substitute (CitraSolv; LLC, Danbury, CT) for 2 – 5 minutes. Tissues were hydrated in a series of alcohols and water before undergoing antigen retrieval by microwaving in 10-mM citrate buffer. After antigen retrieval, endogenous peroxidase activity was quenched with hydrogen peroxide (3% for 10

minutes), and sections were blocked with 10% normal goat serum in phosphate-buffered saline (PBS) for 30 minutes. Primary antibodies were applied for times ranging from 30 minutes at room temperature to overnight at 4°C. Slides were washed twice for 5 minutes each in PBS before application of the secondary antibody. For most antibodies, slides were incubated with the secondary antibodies for 30 minutes then washed several times with PBS. Staining was developed by incubating sections with diaminobenzidine and tissue sections were then counterstained with hematoxylin.

To identify proliferating cells, we used an anti-Ki67 antibody; to assess apoptosis, an anti-activated caspase-3 antibody was used; for sebocyte differentiation, an anti-PPAR gamma antibody was employed. As an alternative method of apoptosis detection, the Frag-EL DNA fragmentation kit from Calbiochem was used as per manufacturer's instructions. All counts were made on multiple sections per animal analyzed and means were compared using Student's t-test.

Hair Follicle Isolation and Flow Cytometry Analysis

Mice were shaved dorsally two days prior to sacrifice. Just before skin collection, Nair was applied to remove remaining stubble. Mice were sacrificed using constant-flow CO₂ followed by cervical dislocation and then the dorsal skin was removed. Fat was removed from the underside of the skin by thorough scraping with a curved-blade razor, and the skin was floated dermis-side-down on 5% (w/v) dispase in DMEM overnight at 4°C. The following morning, epidermis was scraped free from the dermis, and the latter was placed in a dish containing 1% collagenase in DMEM and incubated for ~2 h at 37°C, or until dermal disintegration was evident. Dermal remnants were then

mechanically dispersed by pipetting and centrifuged for 5 minutes. Microscopic inspection revealed intact hair follicles at this stage. 5 mL of 0.25% Trypsin-EDTA was added to the hair follicle preparations for 10-15 minutes until a single-cell suspension was obtained. These cells were then centrifuged at 1,000 rpm for 5 minutes, resuspended in 100 mL of PBS, and incubated with appropriate fluorophore-conjugated antibodies. Flow cytometry was performed on a BD Aria cytometer and all flow cytometry data was analyzed using the FlowJo software program. Population sizes were compared using Student's t-test.

Epidermal Keratinocyte Isolation and Flow Cytometry Analysis

Keratinocytes were isolated from telogen dorsal back skin using thermolysin as described in Jensen *et al* (48). Briefly, the back skin strips were rinsed in 10% Betadine, then PBS, 70% ethanol, and finally again in PBS. The dermal side was thoroughly scraped to remove excess fat, and then the tissue was floated in 0.25 mg/ml Thermolysin (Sigma) in calcium-free FAD medium for ~1 h at 37°C. The epidermis was then scraped from the dermis, minced with dissecting scissors, and dispersed by gentle pipetting. Keratinocytes were further liberated by stirring the epidermal fragments using a magnetic stir bar. Thermolysin was inactivated by adding media containing FBS, and the cells were washed with PBS, then pelleted and resuspended in 100 mL PBS for labeling with antibodies to CD34, integrin $\alpha 6$, Lrig1, or other molecules. Flow cytometry data was analyzed using the FlowJo software, and cell counts were compared using Student's t-test.

Two-Stage Carcinogenesis Experiments

The dorsal skin of 6-8 week old mice in telogen was shaved two days prior to application of 25 ug 7,12-Dimethylbenz(a)anthracene (DMBA) in 200-ml acetone. Two weeks later, and for the 24-week duration of the study, dorsal skin was treated with 12.5 mg 12-O-Tetradecanoylphorbol 13-acetate (TPA) in 200-ml acetone. Papillomas were counted weekly, and carcinomas were evaluated visually and confirmed histologically. Mice were sacrificed prior to the study's completion if the combined tumor burden was excessive, if morbidity was noted, or if a single tumor exceeded acceptable size limits as prescribed by IACUC guidelines. Both female and male FVBs were used in this study, but were never housed together. Moreover, males were housed in small numbers in order to minimize aggressive behavior (none was noted), which could confound tumor data. At the study's conclusion, tumors were harvested, counted, weighed, photographed, and histologically analyzed. Tumor multiplicities were compared using the Mann-Whitney non-parametric rank sum test, while comparisons between tumor incidence were made using the X^2 test. Tumor masses were compared using Student's t-test.

Quantitative RT-PCR Analysis

RNA was extracted using the RNeasy mini kit (Qiagen) with on-column DNase treatment to eradicate contaminating genomic DNA or total RNA was extracted using the miRVana PARIS kit (Ambion), and sample quality was verified using the Agilent Bioanalyzer. Reverse transcription was carried out using the SuperScript III First-Strand Synthesis System (Invitrogen). Real-time primers were designed using NCBI's Primer Blast online software (<http://www.ncbi.nlm.nih.gov/tools/primer-blast/>), and genes to be

analyzed were chosen by culling the literature for ChIP studies in which Nanog binding was assayed. Genes to which Nanog bound near the promoter region in both mouse and human systems were given preference as likely targets of human Nanog protein binding to regions of the mouse genome.

In Vivo Wound Healing Experiments

Epidermal abrasion experiments were performed by shaving mice 2 days prior to wounding. Hair stubble was removed by application of Nair just prior to epidermal abrasion. Mice were anesthetized by inhalation of isofluorane. A felt cylinder was attached to an electric handheld rotary tool, and wounds were made superficially such that the dermis was just visible. Removal of epidermis and integrity of hair follicles were both confirmed histologically on random samples.

In Vitro Wound healing (scrape) assays

Newborn keratinocyte preparations were made by washing P1-P3 pups sequentially in Betadine, alcohol, and water, then sacrificing them using hypothermia. Sacrificed pups were skinned and the tissue floated on 0.25% trypsin without EDTA overnight at 4 degrees C, following which time the epidermis was gently scraped away from the dermis, then minced with dissecting scissors. Additional keratinocytes were dislodged from the epidermal fragments by placing the minced epidermis in a medium-containing dish with a magnetic stir bar and stirring for ~10 min. Keratinocytes were isolated by filtration through a 70- μ m cell strainer or by centrifugation in a Percoll gradient.

The migratory properties of keratinocytes were analyzed using a scrape/wound protocol. Briefly, freshly prepared keratinocytes were plated on collagen-coated dishes in a high-calcium Waymouth's-based (or KBM-Gold) medium and allowed to attach for 4 h. Then the medium was changed to calcium-free KBM Gold supplemented with .05mM calcium carbonate. Cells were allowed to reach confluence and then a pipet tip was used to displace a line of cells along the dish's diameter. Measurements were made 0 and 12 h post-scrape/wound, and images were collected at these time points also. The number of cells that entered the scrape area were counted in each of multiple 40x fields, and the means of the transgenic and wild-type groups were compared using Student's t-test.

Label-Retaining Cell Experiments

Mouse pups were injected intraperitoneally with bromodeoxyuridine (BrdU) twice daily from postnatal day 10 (P10) through postnatal day 12 (P12). Following a chase period of eight weeks, the mice were sacrificed and skin was formalin-fixed and paraffin-embedded for histological analysis and anti-BrdU immunohistochemistry.

Chapter 3- Generation and Characterization of K14. Nanog Transgenic Mice

This project began with the intent of answering a simple question, “Does Nanog play a role in tumor development?” Our studies using various loss-of-function techniques in prostate cancer cell lines suggested that Nanog was a mediator of tumor development. To address these questions in a gain-of-function setting, we first utilized the bovine keratin 5 (BK5) promoter to generate a construct bearing HPCa5T Nanog (NanogP8) cDNA, which was cloned from a primary prostate tumor. Implantation of microinjected embryos bearing this DNA into pseudopregnant females yielded no transgenic founders over the course of over six months and multiple rounds of injection (Table 3-1). Although the keratin 5 promoter should not be active until ~E9.5, circumstantial evidence suggested that expression of Nanog from this time point on was sufficient to cause embryonic lethality in transgenic animals.

We then decided to utilize the human keratin 14 (K14) promoter, which is expressed in the same cell compartment as the BK5 promoter, but is anecdotally known to exhibit relatively reduced expression of the gene of interest. We reasoned that perhaps we would be able to obtain transgenic founders in the absence of dramatic overexpression of Nanog protein. Indeed, after cloning HPCa5T-Nanog cDNA downstream of the K14 promoter (Figure 3-1A), we were successful in obtaining a limited number of founders, four in all, over several months of embryo microinjection and implantation of the embryos into pseudopregnant female mice. Of these potential

Table 3-1

Date of Injection	Number of Embryos Injected	Number of Surviving Embryos	Number of Embryos Transferred	Number of Pseudopregs Transferred To	Number of Pseudopregs Who Became Pregnant	In Utero Harvest (days) Normal Fetuses & Aborts	Number of Pups Born	Number of Transgenics Produced
10/19/06	119	65	65	2	1	N/A	8 live & 2 dead	0
10/25/06	146	90	86	4	3	N/A	13	0
11/2/06	95	64	32	2	0	N/A	0	N/A
11/3/06	82	49	49	2	1	(E17) 5 & 7 abortions	N/A	0
11/9/06	11	83	83	2	2	(E12) 6 & 5 abortions	9	0
11/16/06	94	60	60	2	2	N/A	10	0
12/1/06	101	76	76	2	1	(E13) 5 & 8 abortions	N/A	0
12/8/06	42	31	31	1	1	(E12) 6 abortions	N/A	0
12/13/06	117	78	77	2	2	(E9) 4 & 8 abortions	7	0
1/11/07	95	66	50	2	1	N/A	12	0

Table 3-1 Summary of BK5.Nanog injections

In total, 902 embryos were injected with the BK5.Nanog construct over a course of four months (additional injections were not catalogued but were performed for two additional months), of which 682 embryos survived (and 629 were transferred to pseudopregnant moms). 59 pups were live-born, none of which screened positive for the transgene. Additionally, 26 embryos and 34 “aborts” were harvested, but again no transgenics were produced.

founders, one did not transmit the transgene through the germline, while one mouse that bore a wrinkled skin phenotype died two weeks postnatally. The remaining two founders passed the transgene successfully to subsequent generations and were viable. Line 1 is marked by relatively high Nanog expression as assessed by Western blot, while Line 3 bears moderate transgene expression (Figure 3-2A). Characterization of the lines generated then ensued.

Dose-dependent phenotypes in K14.Nanog mice

Phenotypically, there is a strong correlation between Nanog expression level and severity of the observed phenotype. At the lower levels of Nanog output observed in Line 3, there is no loss of viability and the mice appear grossly normal until about four months of age, at which time they begin to develop cataracts that become bilateral by the time the mouse is six months old. As an aside, Line 3 mice that do not develop cataracts seem to express the transgene more weakly than do those Line 3 mice that possess a lens phenotype (Figure 3-2A). Thus, it is possible that our colony at some point developed a sub-line such that not all Line 3 mice have a propensity to develop cataracts.

Line 1 mice are characterized by perinatal lethality and possible embryonic lethality, with an average litter size of six mice per litter (Figure 3-1C; as compared to the standard of ~10 mice per litter when crossing wild-type FVBs) when hemizygous males were bred to wild-type females (Homozygous transgenic mice were not generated, i.e., hemizygous mice were not crossed due to an expected exacerbation of the reduction in viability). This is consistent with our lack of founders when attempting to generate transgenic mice using the BK5 promoter, and strongly suggests that overexpression of

Nanog at prenatal time points reduces viability. Line 1 mice are much smaller than their wild-type littermates, and this condition persists throughout birth (Figure 3-1D and E). Additionally, Line 1 mice present with wrinkled skin at birth, and as they age they acquire shaggy hair coats (Figure 3-1F). They also possess cataracts, and in this way phenocopy Line 3 mice. However, Line 1 mice develop bilateral cataracts by about one month of age, and exhibit hypophthalmia, or reduced eye size, as well. It should be noted that this line's gross phenotypes seem to attenuate by adulthood, though they are still quite prominent. This effect is compounded by the early death of many transgenic mice; those mice surviving past a critical window of roughly two weeks of age seem to bear less striking phenotypes than those that expire earlier.

We decided to systematically analyze transgenic mice for histological phenotypes that may not be evident to the naked eye, as the keratin 14 promoter is active in a variety of tissues including the skin, forestomach, thymus, and tongue.

Phenotypes-skin

We began by analyzing the skin, as it exhibits the most prominent gross phenotype in Line 1 mice. First, we confirmed proper expression of Nanog according to the expected pattern of keratin 14 expression, and indeed Nanog was localized to basal cells of the interfollicular epidermis as well as to the outer root sheath (ORS) of the hair follicle (Figure 3-1H). We examined mice at P5, rationalizing that observations made in the window prior to extensive perinatal lethality would prove fruitful. Indeed, K14.Nanog mouse skin appears very different than that of wild-type littermates at this time. Whereas wild-type FVB skin shows orderly follicular arrangement, a distinct

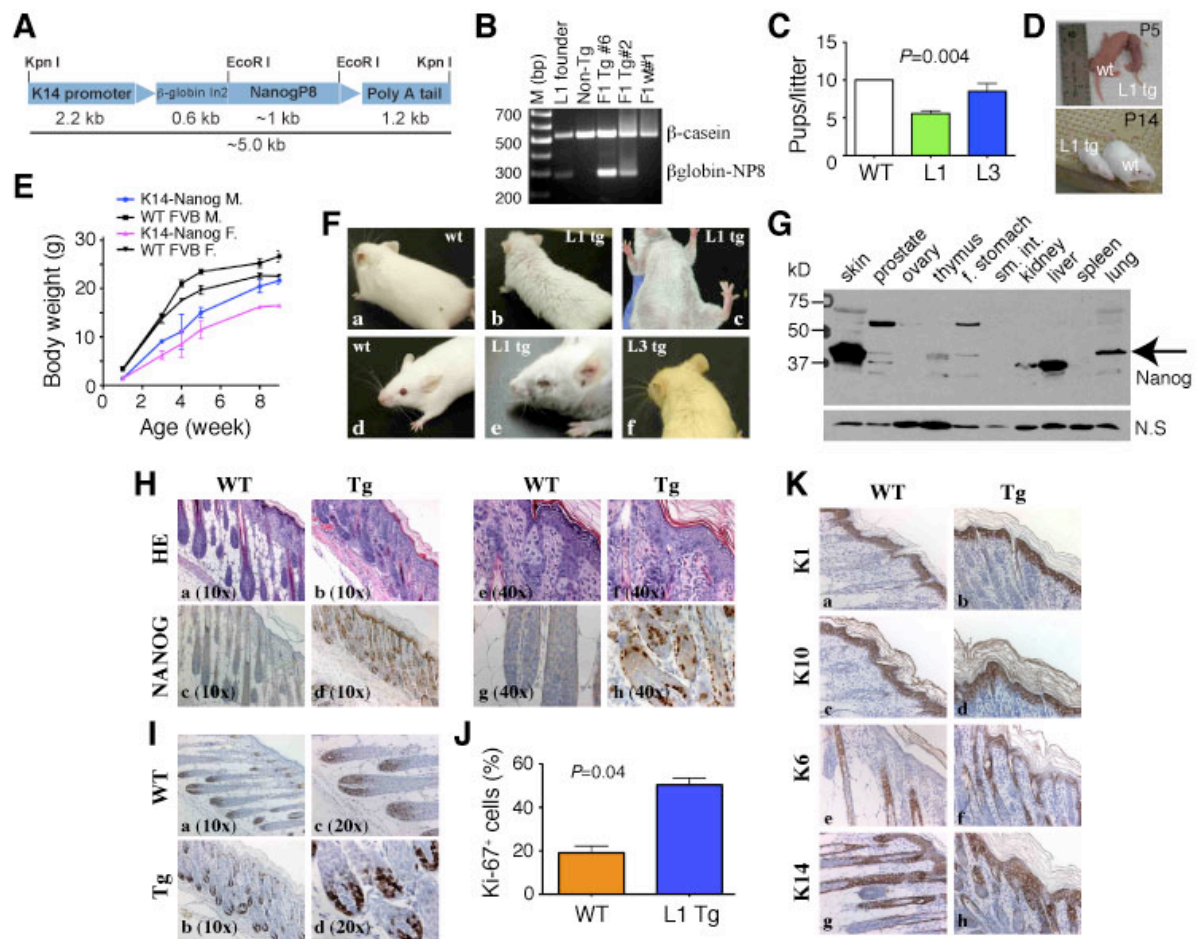
hypodermis, and regularly interspersed sebaceous glands, K14.Nanog mice present with disorganized follicular arrangement, a paucity of sebaceous glands, and the striking absence of a hypodermis (Figure 3-1H).

In order to gain an appreciation for tissue homeostasis at this time point, we conducted Ki67 staining to assess proliferation of the IFE and of hair follicles. Hair follicles are in anagen, the proliferative phase of the hair cycle, at P5, and we confirmed this in both transgenic and wild-type mice. We did find that transgenic mice had a noticeable increase in proliferation of the basal cells of the IFE relative to wild-type mice (Figure 3-1I and J), although this difference seems to abate by 2.5 weeks of age (Figure 3-3G). This finding is augmented by the presence of keratin 6-positive cells in both the IFE and the ORS of the hair follicle of transgenic mice, but only in the ORS of wild-type mice (Figure 3-1K), as keratin 6 is considered to be a marker of activated or proliferating epidermal cells (59). As tissue homeostasis is a balance between the appearance of new cells through proliferation and the loss of existing cells, which may occur through cell death or differentiation, we wondered at the fact that there was no visible difference in epidermal thickness between Line 1 and wild-type mice. To address this enigma, we performed IHC staining for suprabasal markers of IFE differentiation including keratins 1 and 10 (Figure 3-1K). We found a slight increase in K1/K10 in transgenic mice, which coupled with no detectable difference in apoptosis as assessed by TUNEL staining suggests that epidermal hyperplasia was not seen as these cells were following the normally-prescribed route of differentiation as they ascend. However, we did note abnormal differentiation of the sebaceous gland population, one of the three primary epidermal lineages. As mentioned previously, transgenic mice

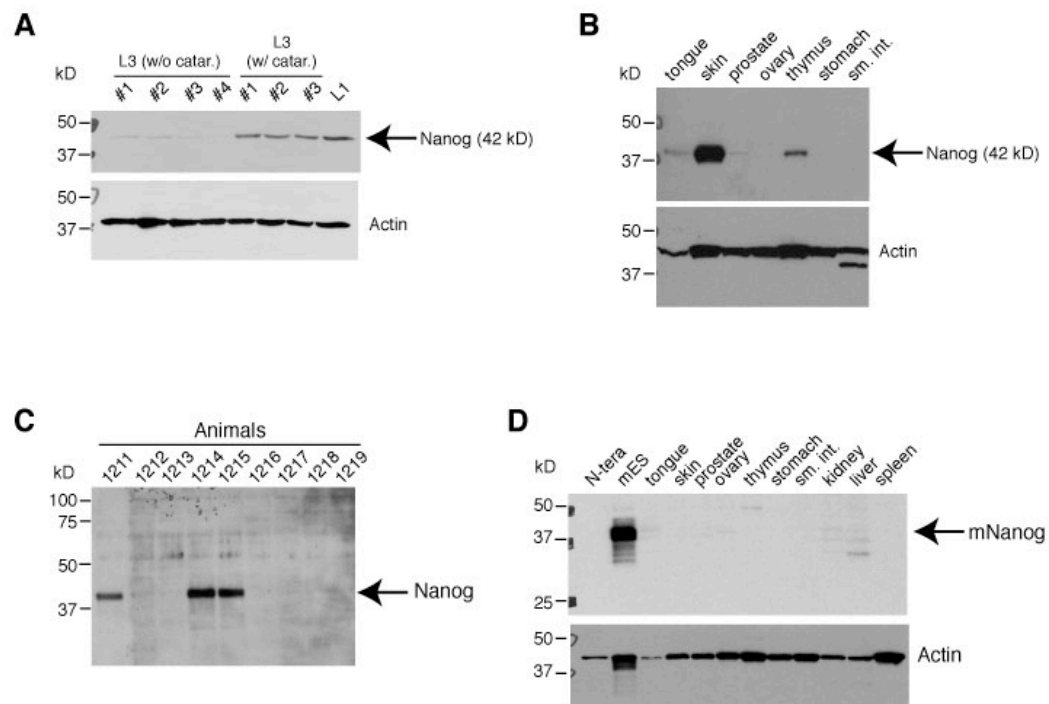
possess significantly fewer sebaceous glands than their wild-type littermates; this is evident both in hemotoxylin and eosin sections and in PPAR-gamma IHC images (Figure 3-3B and C).

Wound healing defect in K14.Nanog mice

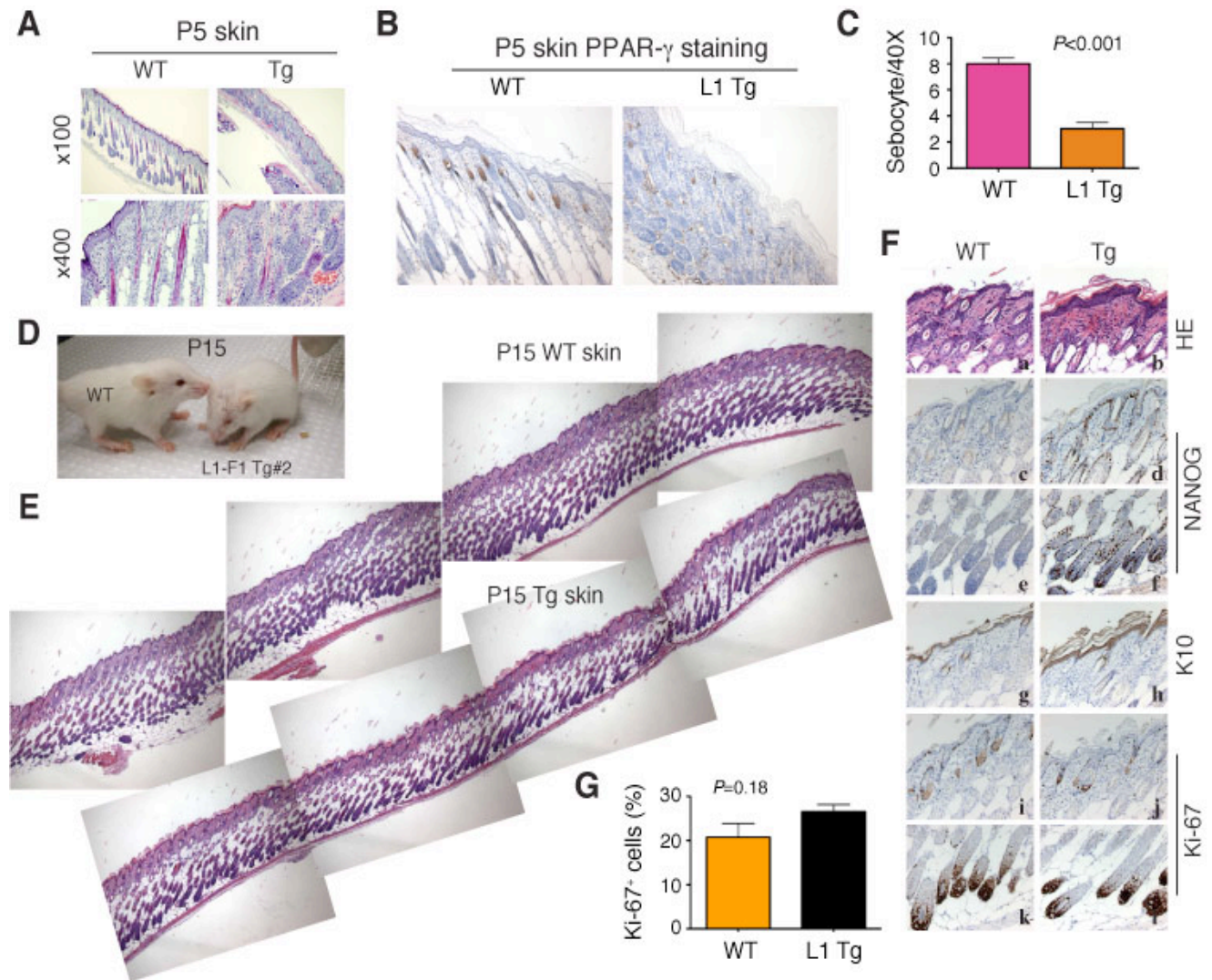
During the course of our passive assessment for spontaneous tumor development, which lasted upwards of 1.5 years, we noticed that adult K14.Nanog Line 1 mice developed extensive wounding on the skin covering their ears; this occurred in the absence of pugilism with littermates. As it was unknown whether this was behavioral in nature, i.e., the mice were inflicting repeated mechanical stress/damage upon themselves, or whether these wounds were arising spontaneously as has been reported in some transgenic models (60), we conducted formal wound healing experiments by abrading the epidermis with a felt wheel and assessing the regrowth of the removed area. K14.Nanog mice exhibited little re-epithelialization of the affected area, whereas wild-type mice showed complete re-epithelialization within a week of abrasion (Figure 3-4A). It became apparent that wounds inflicted on the transgenic mice were not healing from inside the wound proper, but instead contraction of the bordering epithelium could be observed. Langton and colleagues demonstrated that such auxiliary wound healing occurs in the absence of a contribution from the hair follicle (61), which we suspected to be the case in our wound healing system. As an aside, it appeared that transgenic mice were more sensitive to the touch following wounding, and the exposed wounds themselves bore a gross inflammatory character including redness along the wound

Figure 3-1**Figure 3-1 Characterization of K14.Nanog transgenic mice**

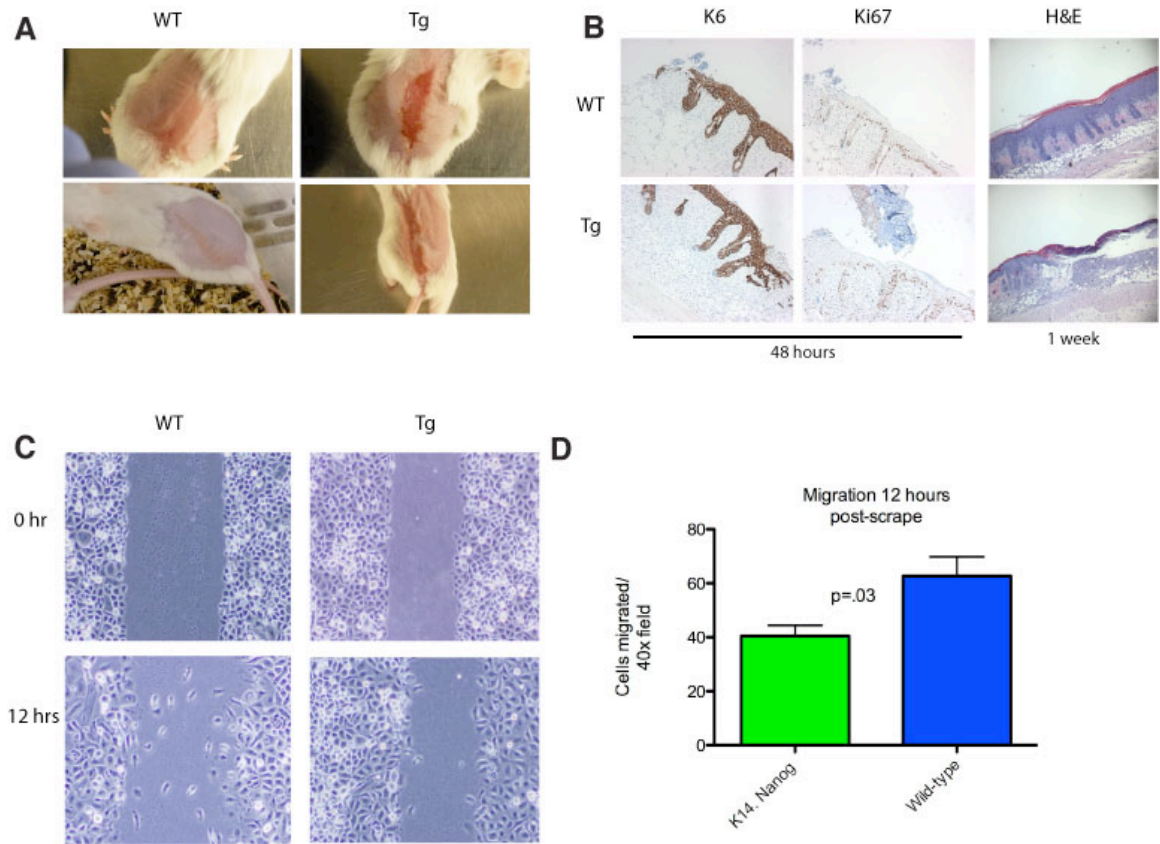
HPCa5T-derived Nanog cDNA was cloned into the human keratin 14 vector to create the construct depicted in (A); transgenic mice were screened for using PCR as depicted in (B). Line 1 (L1) litters are much smaller than those of Line 3 or wild-type FVBs (C). The L1 mice themselves are smaller as well; this condition persists from birth throughout adulthood (D and E). The most obvious adult phenotype is in the skin of L1 mice, which bear curly whiskers and shaggy hair (F). Expression of Nanog protein in Line 1 mice is, as expected, strongest in the skin and absent in tissues lacking a keratin 14 cellular compartment (G). Analysis of the prominent skin phenotype in Line 1 mice at P5 (H-K).

Figure 3-2**Figure 3-2 Nanog protein expression in transgenic mice**

Line 1 mice bear the strongest levels of Nanog expression in the skin as assessed by Western blot (A) and (C). Note that Line 3 mice that harbor cataracts seem to express more Nanog protein than transgenic mice that lack a gross phenotype. Depicted in (B) is a systematic analysis of Nanog levels in keratin 14-expressing organs. Skin, as expected, expressed the transgene more robustly than the other tissues. Wild-type mice do not express mouse Nanog protein in any organs analyzed (D).

Figure 3-3**Figure 3-3 Characterization of Line 1 skin abnormalities**

K14.Nanog mice (Line 1) lack a hypodermis, have disorganized follicular placement, and have relatively few sebocytes (A-C); the abnormalities in the skin are manifest grossly as shown in (D). By two weeks of age, the hyperproliferative phenotype has abated although transgenic skin is not identical to that of wild-type littermates histologically (E-G).

Figure 3-4**Figure 3-4 K14 Nanog mice exhibit a wound-healing defect**

Epidermal abrasions heal more slowly in K14. Nanog mice than in wild-type FVBs (A). In addition, the wounds tend to heal from without rather than from within the wound. Markers of activated (keratin 6) and proliferating (Ki67) epidermis do not vary between the two groups after two days' time, although the degree of overall healing by one week does (B). *Ex vivo* keratinocyte scrape assays suggest that keratinocytes derived from transgenic mice are less capable of migrating through an artificial wound than are wild-type FVB-derived keratinocytes (C and D).

margins. This suggests that the abrasions may cause a more pronounced inflammatory response in transgenic mice than in wild-type controls. To better understand the observed disparate responses to epidermal abrasion, we assessed the short-term activities of the affected skin population histologically. In both wild-type and transgenic mice, the short-term wound healing proliferative response as assessed by Ki67 was intact (Figure 3-4B). Expression of keratin 6, a marker of activated epidermal cell populations that partners with keratin 16, was identical 48 hours post-wounding as well (Figure 3-4B). Expression of both of these keratins is essential for cells to properly migrate through the wound area (62). H&E staining at 7 days post-wounding clearly shows that wild-type wounds are almost fully re-epithelialized, while transgenic dorsal skin shows a discontinuous epidermis and scabbing (Figure 3-4B).

We wondered if transgenic keratinocytes could migrate properly in response to wounding, and to address this issue, we employed an *ex vivo* assay in which keratinocytes derived from newborn pups were allowed to reach confluence, after which time a scrape was made through the sheet of cells; this is the artificial “wound”. We observed migration of wild-type and transgenic keratinocytes following the “wounding,” and found that fewer transgenic keratinocytes were able to enter the wound at 12 hours post-scrape than were wild-type cells (Figure 3-4C and D).

Phenotypes-lens

We then sought to understand the nature of the shared phenotype between Lines 1 and 3 in the ocular lens. It should be noted that the lens is not a keratin-14 expressing cellular compartment, but several transgenic models utilizing the artificial human keratin

14 promoter to drive expression of human papilloma viruses noted cataract formation (63, 64); it is likely, therefore, that the human keratin 14 promoter is missing regulatory elements such that transgene expression occurs aberrantly in the lens. In a normal lens, epithelial cells migrate posteriorly toward the bow or ribbon region near the equator, and as they do so they begin to enucleate and express early differentiation markers such as p57 and later markers such as the various crystalline proteins that allow the lens its unique optical properties.

In the K14.Nanog transgenic lens, this pattern is altered, as nucleated cells are found posterior to the lens equator, and vacuolated cells are present within the lens as well (Figure 3-5B and D). The presence of bladder-shaped cells in lieu of normal lens epithelial cells suggests an altered cell fate, which we confirmed by staining for beta-crystallin (Figure 3-5E). The presence of alternate cell types disrupts the normal lens architecture such that the lens becomes opaque; it is likely also that cell-cell interactions that serve to stabilize the overall lens architecture are abnormal as well, and that this may be a contributing factor to the cataract phenotype. In Line 3 animals this process is gradual and occurs over roughly six months in a Nanog dose-dependent fashion, while in Line 1 animals cataracts are evident from as early as one month.

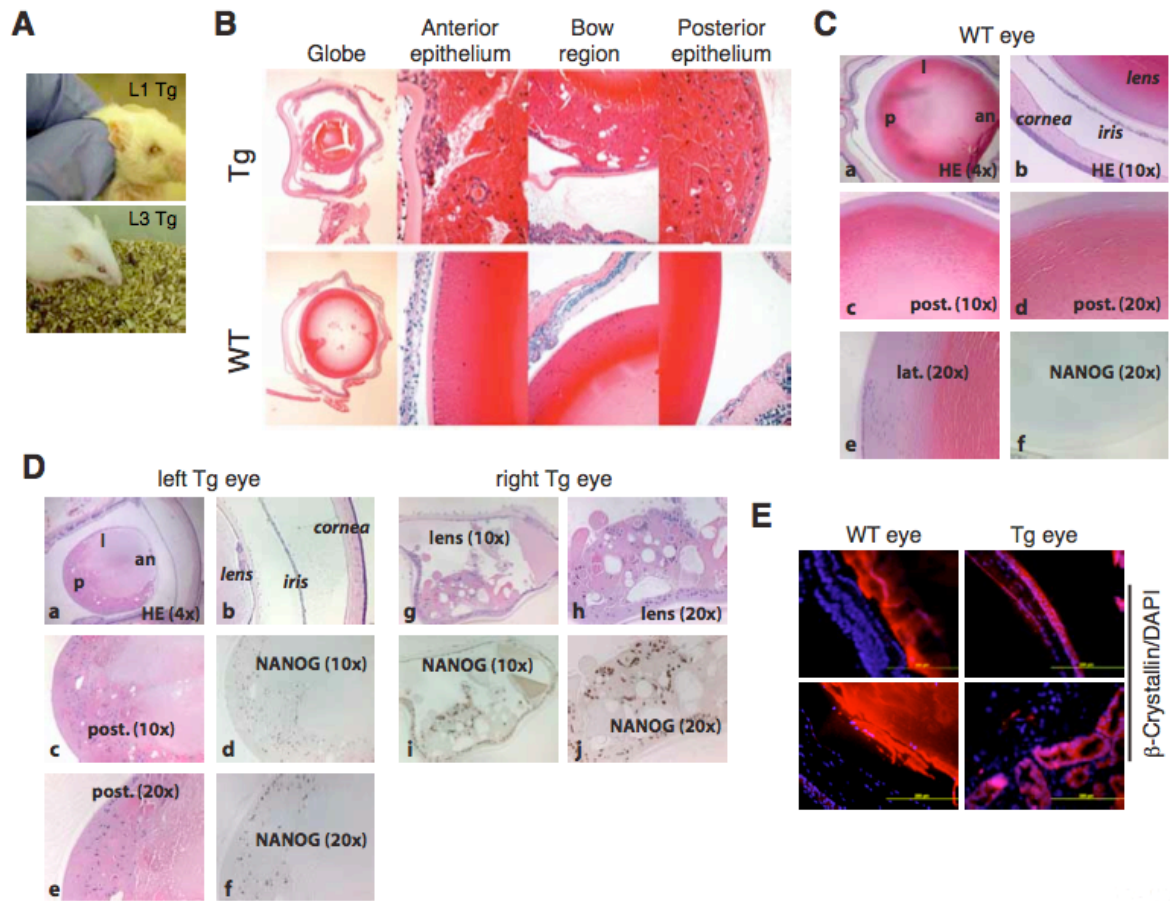
Phenotypes-lingual/digestive

We were interested in the digestive processes of transgenic mice, as they appeared to feed poorly at perinatal time points, often possessing small or absent milk spots. The stomachs of wild-type mice were quite full, but oftentimes transgenic mouse stomachs were bereft of food, and as such had thickened adluminal epithelial layers

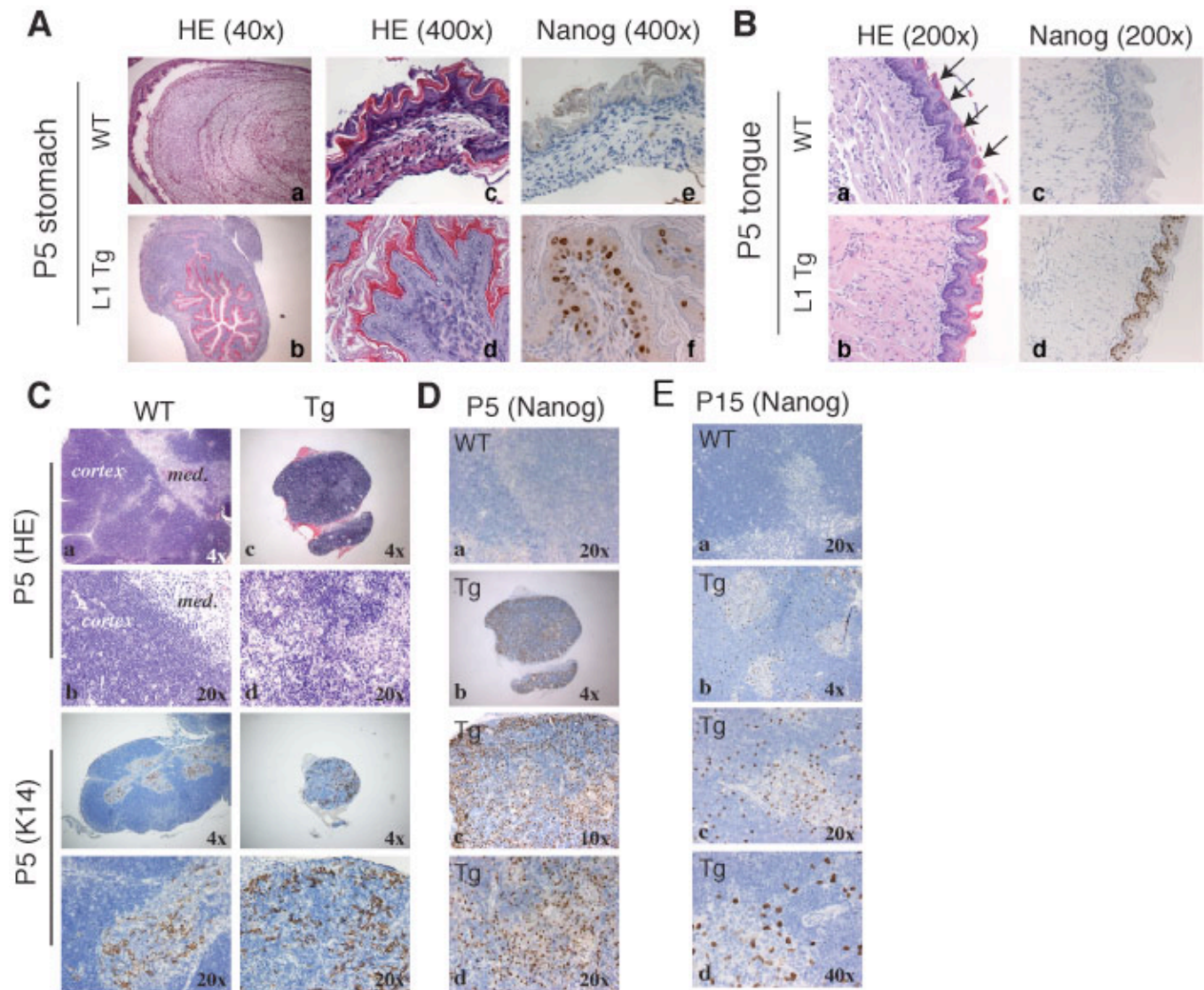
(Figure 3-6A). We then analyzed the tongue for any possible abnormalities. H&E staining shows that transgenic tongue is wrinkled and hyperkeratinized relative to that of wild-type littermates (Figure 3-7A). Microscopic examination revealed a striking lack of filiform papillae, the most abundant of the four types of lingual papillae that are found on the dorsal surface and in which taste buds are located, in the tongues of P5 and two-week-old transgenic mice (Figures 3-6B and 3-7B and C). We also noted a reduction in the level of keratin 13, a marker of a differentiated lingual epithelium layer, and a disruption of the normal stratified epithelial organization, again suggestive of a series of inappropriate differentiation events (Figure 3-7E).

Phenotypes-thymus

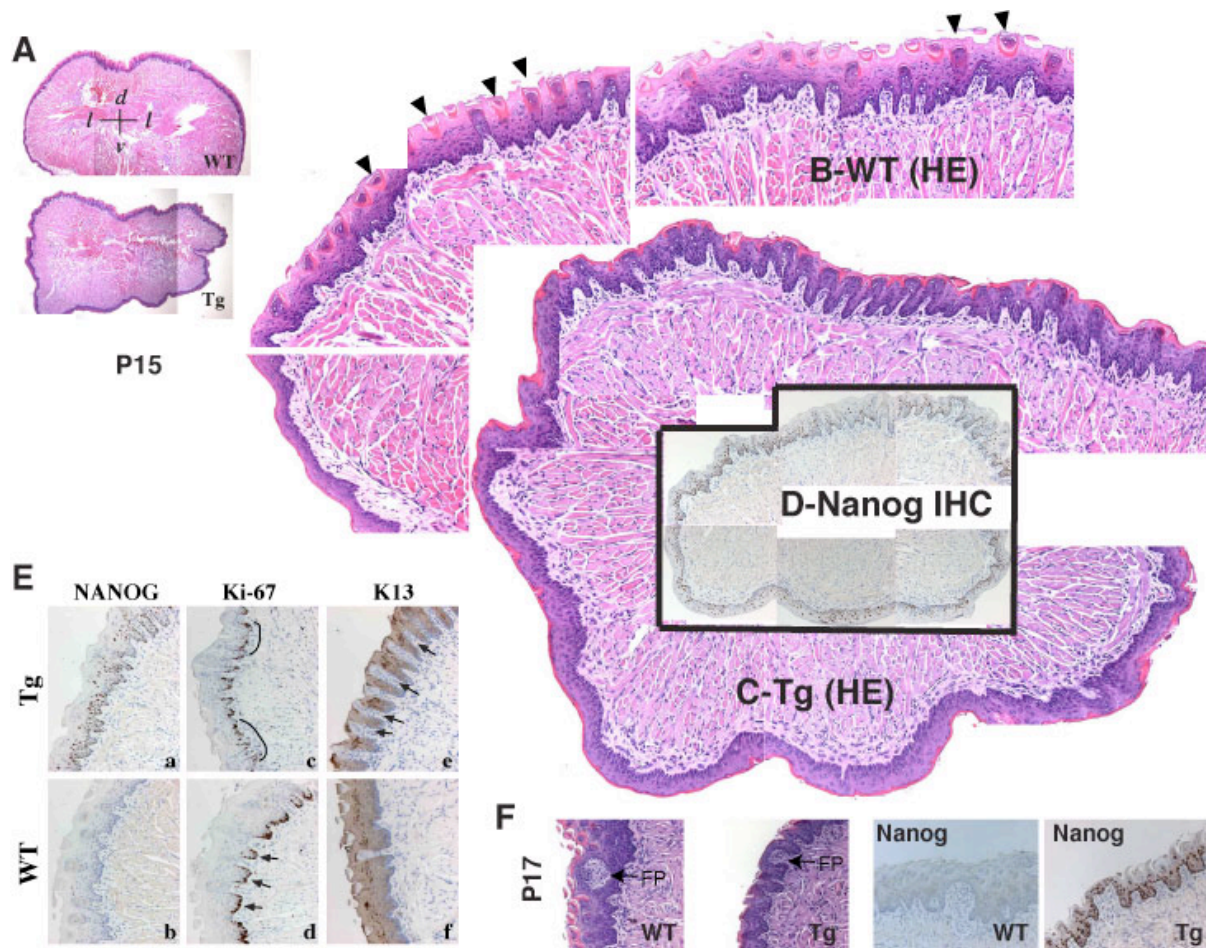
In cataloguing the developmental abnormalities in various keratin 14-expressing organs, we noticed a striking thymus phenotype. The thymus in K14.Nanog transgenic mice at P5 is much smaller than that of wild-type littermates, even when these numbers are normalized to account for differences in body mass. Even more prominent is the lack of delineation between the medullary and cortical regions of the thymus; this lies in stark contrast to the well-ordered boundaries between the two in wild-type thymii of age-matched controls (Figure 3-6C-E). As it is known that the medulla is formed by the expansion of progenitor cells to form islets, and that these islets coalesce to form the structure we recognize as the medulla proper (65, 66), it is reasonable to speculate that the apparent lack of segregation between the cortex and the medulla in transgenic mice may in fact reflect an inability of the progenitor cell population to undergo this requisite expansion.

Figure 3-5**Figure 3-5 Shared lens phenotype between Line 1 and 3 transgenic mice**

Cataracts are evident in both Line 1 (by 1 mo) and Line 3 mice (by 4-6 mo) (A). Histological analysis of transgenic eyes shows nucleated cells at the posterior region of the lens of K14. Nanog mice (B). Vacuolated cells and bladder cells are evident in tg eyes also (B and D). B-crystallin staining shows reduced expression of this terminal differentiation marker in tg eyes (E).

Figure 3-6**Figure 3-6 Characterization of Digestive and Thymic Ancillary Phenotypes at P5**

Transgenic mice often lack a milk spot at early perinatal time points; this finding is confirmed by the absence of food in the stomach of tg mice, which in part leads to a hyperkeratinization phenotype in the epithelium bordering the lumen (A). Because of this finding, we examined the lingual epithelium of wild-type and K14. Nanog mice and found an absence of filiform papillae (B) that is not rescued by two weeks of age. An unrelated phenotype is found in the thymus, which in transgenic mice is disproportionately smaller than in wild-type mice and bears a lack of distinction between cortical and medullary regions (C,D,E).

Figure 3-7**Figure 3-7 Abnormal differentiation in SSE of K14. Nanog tongue**

K14.Nanog tongues appear grossly wrinkle and hyperkeratinized relative to those of wild-type littermates (A). Incredibly, they also lack to a large extent the filiform papillae, differentiated taste bud structures derive from the stratified squamous epithelium (B and C), but retain fungiform papillae (F). Regions of hyperproliferation corresponding to Nanog (+) cells can be observed, and staining for the differentiation marker keratin 13 staining presents abnormally as compared to wild-type littermates (E).

Chapter 4- Testing Nanog's Effect on Tumor Development

Lack of tumor development in K14.Nanog mice

The thought that germinated this project is that Nanog plays a role in tumorigenesis, but after over a year-and-a-half of passive observation, we observed no gross tumor formation that was attributable to Nanog expression in the keratin 14 cellular compartment. This suggests that Nanog expression in keratin 14-expressing epithelia alone is not sufficient to drive tumor formation. We therefore employed methods known to produce tumors in hopes that we would see a perturbation of these tumor phenotypes in K14.Nanog animals.

First, we crossed our K14.Nanog mice with K5.Myc mice in which c-Myc was robustly expressed in the keratin 5 cellular compartment. These mice are known to develop spontaneous tumors in the skin and mouth (67), and as such provide a platform for us to study the role of Nanog in a setting known to foster tumor development, one in which a known oncogene is co-expressed. We crossed both of our existing lines of K14.Nanog mice with K5.Myc mice, but were surprised to find that we could not recover double transgenic mice (Table 4-1); shortly thereafter we abandoned these crosses as our data suggests that expression of both of these molecules prenatally may result in embryonic lethality.

As an alternative to breeding schemes that would favor tumor development, we rationalized that we could observe Nanog's impact on several well-defined parameters of tumor development in a two-stage skin carcinogenesis model. In this model, initiation and promotion are separate entities that can be studied apart from one another.

Table 4-1**K14.Nanog x K5.Myc**

litter	Date of birth	Number of pups	Line	Double-positive pups expected	Double-positive pups obtained
1	9/25/08	6	1	1.5	0
2	9/29/08	3	3	.75	0
3	10/7/08	6	3	1.5	0
4	10/27/08	3	3	.75	0
5	10/30/08	4	1	1	0
6	11/26/08	4	3	1	0
7	12/30/08	6	1	1.5	0
8	1/6/09	4	3	1	0
9	1/12/09	10	3	2.5	0

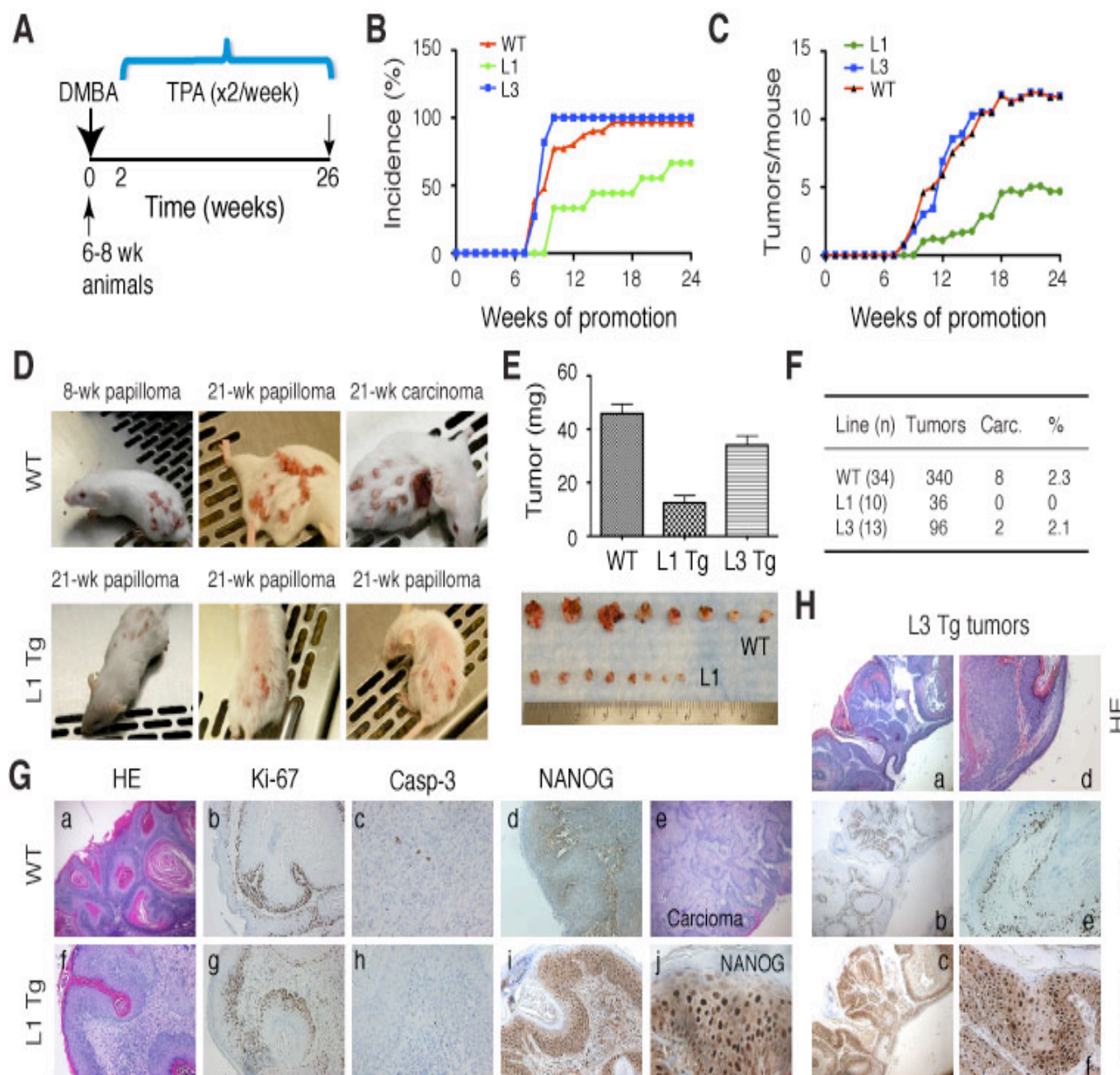
Table 4-1 K14.Nanog/K5.Myc breedings failed to yield double-transgenic pups

K14.Nanog mice were bred to K5.Myc mice for a period of four months with the expectation that adult mice bearing both transgenes would develop tumors at a higher rate and with a shorter latency than K5.Myc mice. However, double transgenic mice were not obtained, even though a dozen mice would be expected to be liveborn were these breedings proceeding according to Mendelian ratios.

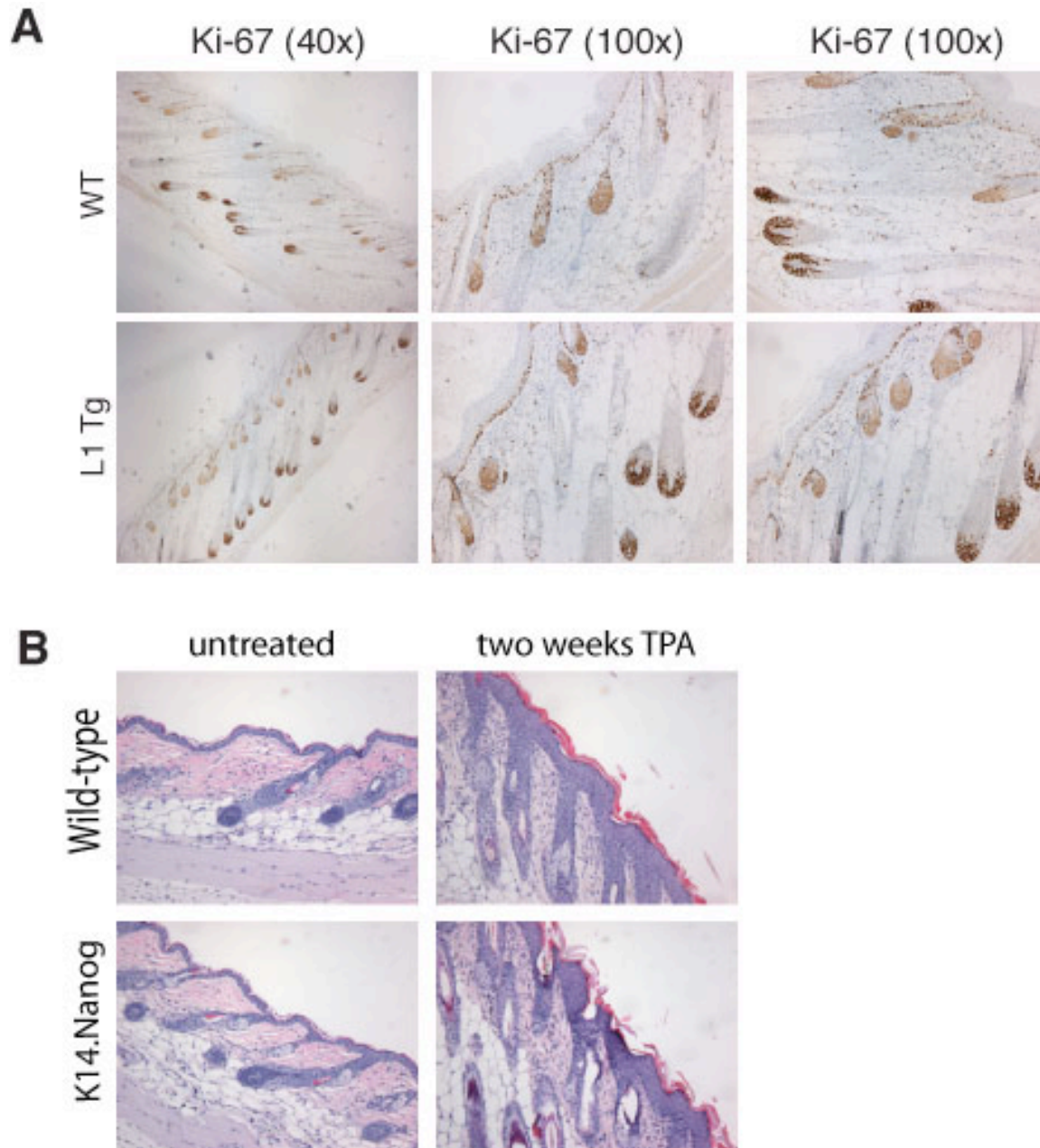
We began this protocol with a two-fold working hypothesis: Either 1) Nanog expression may expand the stem/progenitor compartment (as evident in the aforementioned Oct4-inducible transgenic model) and therefore increase the number of potential carcinogen targets, with the outcome being a higher tumor burden or 2) Nanog may operate more as a classical oncogene, increasing the rate of cellular proliferation (as we observed in our P5 skin analyses) and therefore shortening tumor latency. We were therefore puzzled when it became apparent that Line 1 K14.Nanog mice were developing fewer tumors than their wild-type and Line 3 counterparts (Figure 4-1B and C), and that these tumors were appearing later (at 10 weeks rather than ~8 weeks) as well. Even more surprising was the nature of the tumors themselves: Whereas papillomas arising in wild-type mice were fairly robust at about 40mg/tumor and appeared partially vascularized, tumors arising in Line 1 mice were almost one-third the size and seemed dessicated (Figure 4-1E and H). Unsurprisingly, Line 1 tumors did not, over the course of the 24-week TPA treatment, become endophytic and progress to SCCs, whereas wild-type and Line 3 papillomas did so at a predictable and nearly identical rate (Figure 4-1D and F).

We explored a number of potential causes for these dramatic differences, first dissecting the carcinogenesis protocol into its constituent steps in order to determine where potential discrepancies may lie. First, we examined the consequences of DMBA application by assessing apoptosis 48 hours after administration of the initiating agent. We conducted TUNEL staining to address this issue and found no discernible difference between wild-type and transgenic mice. As a further control, we tested Protein Kinase C levels in both wild-type and transgenic animals, as PKC activation underlies the bulk of

the proliferative response to TPA; we found no noticeable difference between the two groups. We then examined the promotion step of the two-stage protocol; specifically, we wanted to see if transgenic and wild-type epidermis proliferated in a similar fashion when treated with repeated (every other day for two weeks) doses of TPA. Proliferation, as assessed by Ki67 staining, was similar, and both groups exhibited the expected epidermal thickening and hyperplasia in response to the two-week TPA regimen (Figure 4-2A and B). We therefore concluded that a short-term response to neither the initiating nor promoting agent was impeding papilloma development.

Figure 4-1**Figure 4-1 Two-stage skin carcinogenesis**

Mice were initiated with 25ug of DMBA and, after two weeks' time, lesions were promoted with twice-weekly applications of TPA for a period of 24 weeks (A). Line 1 transgenic mice did not uniformly develop tumors, though Line 3 and wt mice did (B). In addition Line 1 mice displayed a much lower tumor burden than the other groups (C, D). The papillomas that did arise in Line 1 mice were runted and did not convert to carcinomas (F). Histological characterization of tumors arising from all three groups (G,H).

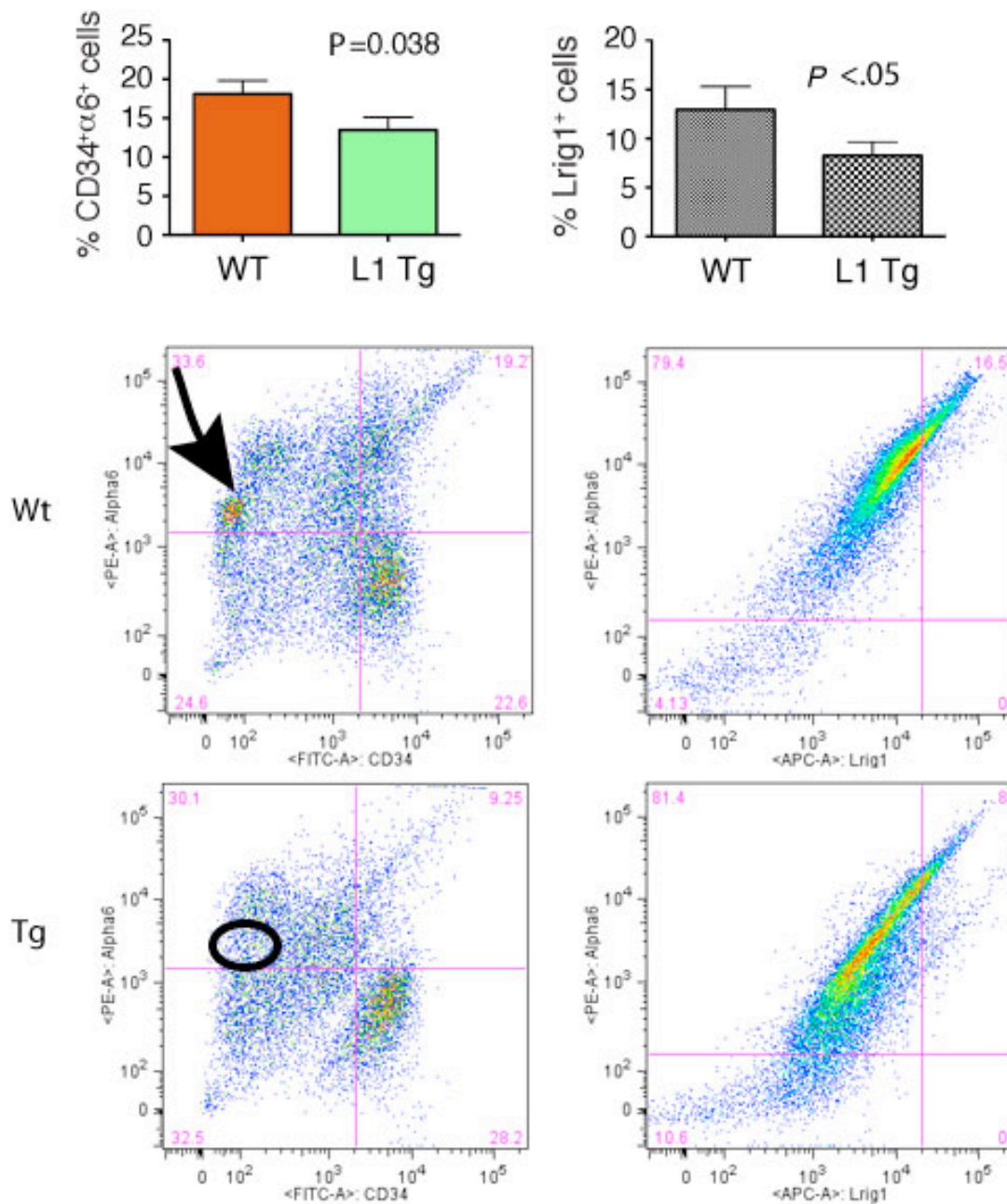
Figure 4-2**Figure 4-2 Hyperplastic response to TPA treatment**

Both wild-type and transgenic mice show increased Ki67 staining after two weeks of treatment with the tumor promoter TPA (A). This is accompanied by a pronounced hyperplasia in the IFE of FVB and K14.Nanog mice (B), suggesting a similar proliferative response to TPA between the two groups.

Chapter 5- Analysis of Skin Stem Cell Populations and Epidermal Gene Expression

Assessment of skin stem cell populations

We reasoned that the inhibition of skin tumor development seen in K14.Nanog mice may be linked to the failure to repair epidermal wounds. Both processes require the presence and participation of resident stem cell populations (54, 55, 68, 69), so we isolated hair follicle keratinocytes and analyzed their cell surface marker profiles to look for intact stem cell pools (depicted in Figure 1-2). We first examined the classical CD34⁺, alpha6 integrin⁺ stem cell pool, as it is widely regarded as the most crucial and primitive of the resident skin stem cell populations. We found that K14.Nanog skin harbored fewer bulge stem cells than age-matched wild-type FVB mice, although the cause of this is not immediately apparent (Figure 5-1). Strikingly, however, we noted the apparent diminution of a CD34^{low} alpha6 integrin^{intermediate} population in transgenic animals. This population most likely lies above the region of CD34 positivity, and therefore resides closer to the epidermis. This finding, along with our observations in P5 skin that the IFE is hyperproliferative while sebaceous glands are scarce, suggested to us a potential loss of Lrig1⁺ stem cells. We therefore isolated epidermal keratinocytes using thermolysin instead of trypsin to avoid cleavage of the relevant epitope, and discovered that the Lrig1⁺ population was diminished in transgenic mice (Figure 5-1). Since the IFE has a resident stem cell pool of slow-cycling cells, we used the label-retaining method to identify IFE LRCs by pulsing wild-type and transgenic mice with BrdU and chasing for 6 weeks. Transgenic IFE contained only one-half the number of

Figure 5-1**Figure 5-1 Diminution of hair follicle stem cell pools**

Keratinocytes were isolated from hair follicles (for CD34, CD49f analysis) and from epidermis (for Lrig1 analysis) of two month old wild-type and transgenic animals. Wild-type hair follicles seem to possess a CD34^{low}CD49f^{intermediate} population that is lacking in transgenic mice (arrow-wt, hollow circle-tg).

label-retaining cells as wild-type epidermis, although their rates of proliferation seemed to be roughly equivalent.

Although we have observed apparent migration impediments and a diminution of the resident stem cell pools in the skin of K14. *Nanog* mice, we did not have an explanation at the level of molecular resolution. We therefore asked, “Which genes might *Nanog* be affecting to bring about the observed phenotypes?” To answer this question, we combed through published studies (14, 70-73) in which *Nanog* binding to gene promoter regions was assayed. Because our transgenic model involves expression of human *Nanog* in a murine system, we selected those genes whose promoters were bound by *Nanog* in both mouse and human studies. These conserved targets, we reasoned, may be preserved in our artificial system. We chose 23 genes that fit our criteria and designed primers (which spanned introns when possible) for SYBR-green-based qPCR analysis (Table 5-1; only specific and amplified targets presented). We then extracted total RNA from cryopulverized mouse epidermis of each transgenic and wild-type mice and carried out real-time PCR (results displayed in Figure 5-2).

As is often the case in Science, much of our resulting data was inconclusive, with no clear distinction between transgenic and wild-type expression levels. In some cases, no amplified product was observed, suggesting a lack of expression of that particular gene in mouse skin. This group includes *Sox2*, a finding that is unsurprising given that it is chiefly found in the pluripotent embryo. There were, however, a number of targets whose altered expression may explain in part the skin phenotypes we observe; the most prominent and exciting of this group is the mouse homolog of c-Jun, the subunit of the AP-1 transcription factor. This protein is widely recognized as a proto-oncogene and

has prominent roles in skin proliferation, wound healing, and inflammation. We performed IHC staining for c-Jun and found that c-Jun seems to be expressed more weakly in transgenic animals. Additionally, Nanog and c-Jun expression is mostly exclusive, that is, they do not overlap to any substantial degree (Figure 5-3). One highly relevant study demonstrated that a transactivation mutant of c-Jun, one that effectively reduced the concentration of Ap-1 able to function transcriptionally, was able to impede papilloma development in a two-stage protocol (DMBA/TPA) but was unable to block TPA-induced proliferation (74). This is essentially the phenotype we see when we subject our K14.Nanog mice to a two-stage carcinogenesis protocol.

I am unsure if this diminution of c-Jun levels is direct or indirect, however. Although large-scale ChIP-seq studies have demonstrated that the c-Jun promoter may be a target for Nanog binding, there exists the very small possibility that this promoter is among those inevitable false-positive results inherent in such large-scale genome analyses. Additionally, the binding may be authentic yet there may be no relevant repressive activity directly exerted by Nanog. It is also possible that Nanog binding to the promoter prevents other transcription factors from occupying certain regions upstream of the transcription start site, and thus a direct repressive effect may exist. This can be experimentally tested by conducting an immunoprecipitation (IP) experiment using epidermal lysate. Immunoprecipitating Nanog will probably result in the pull-down of associated proteins, and the authenticity of these interactions can be confirmed by performing a reciprocal IP. A final possibility, owing in no small measure to the complexity of transcription factor gene expression networks, may be that lowered c-Jun levels are simply an indirect consequence of Nanog expression in the skin, a locale from

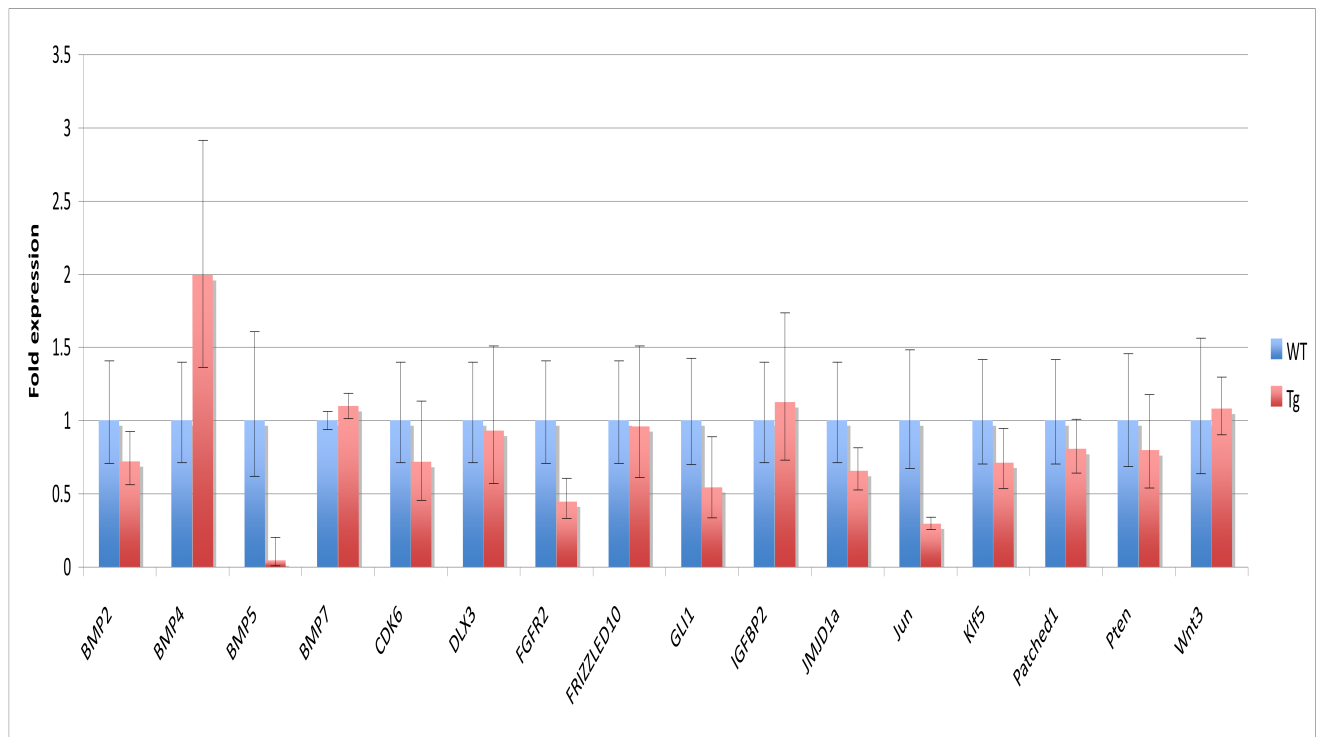
which it is normally absent, although the fact that Nanog and Jun seem not to colocalize, i.e., Jun seems absent or low in Nanog-positive cells argues against this.

Another potentially exciting finding is that the lower levels of Bmp5 in the epidermis of transgenic mice may explain in part our apparent stem cell depletion. A study published in 2011 from the Morris lab showed that Bmp5 levels are strongly correlated with and directly proportional to *ex vivo* colony formation and *in vivo* label-retaining cell number (75). Additionally, we have identified fibroblast growth factor receptor 2 (Fgfr2) and Jmjd1a (a well-known lysine demethylase) as downregulated genes in K14.Nanog epidermis, but have yet to follow up on the potential significance of these finding. It is likely, of course, that our screen has failed to identify some genes that are causally related to the skin phenotypes we have observed, and that ascribing one gene to each observed phenotype is a dramatic oversimplification.

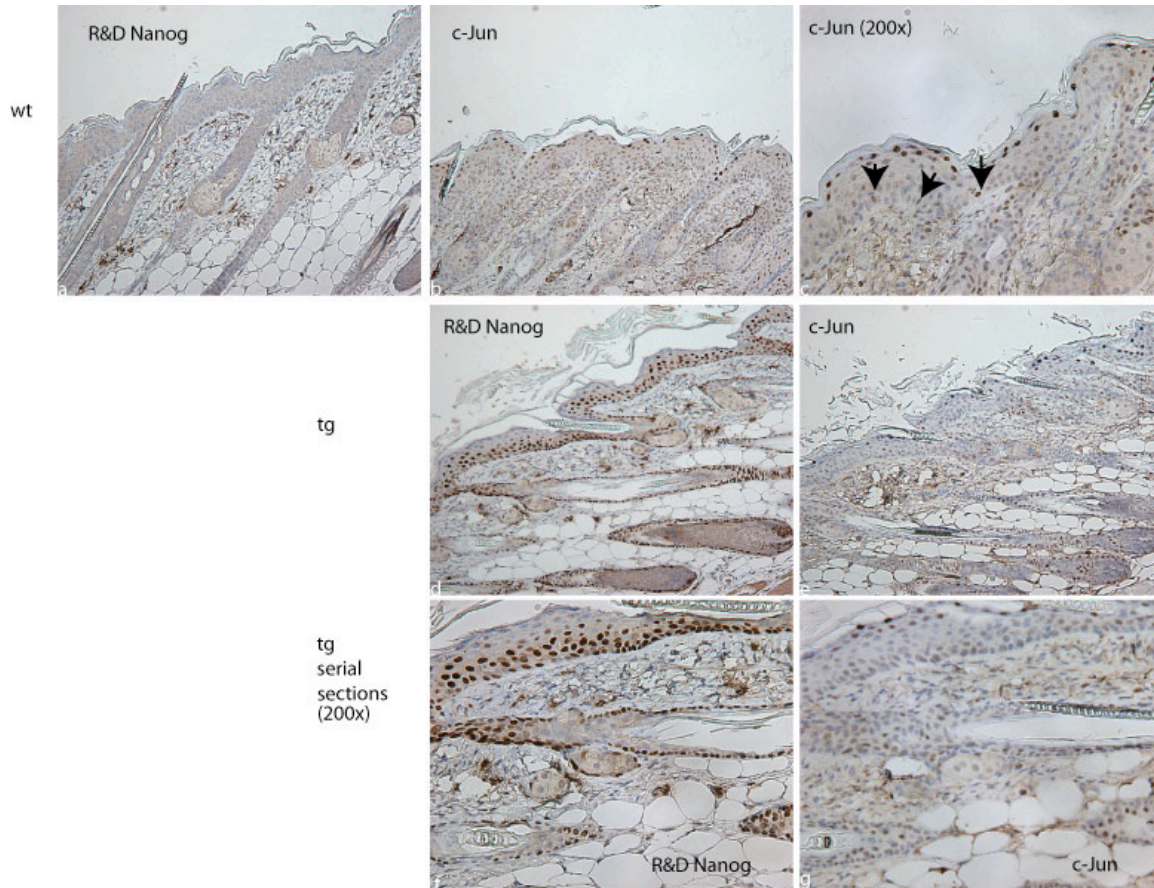
A close inspection of our qPCR data shows that target genes seem to be, on the whole, repressed rather than elevated in transgenic mice (refer again to Figure 5-2). This may reflect a direct repressive event, such as the reported binding of Nanog to Smad1, which blocks bone morphogenic protein (BMP) signaling (76), or an indirect repressive event, such as Nanog occupation of promoters impeding normal binding of endogenous transcription factors.

Table 5-1 Primers used in epidermal gene expression studies

Gene	Forward Primer (5'–3')	Reverse Primer (5'–3')	Product Size	Annealing Temperature
BMP2	TCCAGAGCTGGGCCGAAGA	GAAGAAGCGCCGGCCGTTT	322bp	60
BMP4	TGCCATTCGGAGCGACGCAC	CGCGTGGCCCTGAATCTCGG	244bp	60
BMP5	GCCTCTCCAATGGGTATGCGC	TGCTTCTCCATGTGGAATCTGGGT	225bp	58
BMP7	CGGACAGGGCTTCTCTACCCC	AACCGGAACTCCCGATGGTGGT	177bp	60
Cdk6	CACGGACGGACAGAGAAACCAAGC	CACAGCGTGACGACCACCGA	295bp	59
Dlx3	TACTCGGGCCAGCCCTACGG	CGTTCGCGGCTTTCGGACCT	252bp	59
Fgfr2	CCAGGGATTGGCACTGTGACCA	ACTGCAACTCTAGCGATTCCCCG	205bp	58
Frizzled 10	GGTCACGAGAACCAGCGCGA	ATCCGAGCCGTTGTTGGGTGC	300bp	59
Gli1	AGACGCACCTTCGGTCGCAC	CCCCTCGATGCCGCTTGGTC	243bp	59
Igfbp2	CGCTACGCTGCTATCCCAACCC	GGTCCAACCTCTGCTGGCAAGG	363 bp	59
Jmjd1a	TCCCAGGCAGCCAATTCTCCA	TGGCTGTGGAGCAGACTCCAGT	274bp	59
Jun	GACGGACTTGCCAAACCCGG	GCAAAAGTTCGCTCCCGGCC	292bp	59
Klf5	CCCACCTCCGTCTATGCCGC	GCGGGTCAGCTCATCCGACC	298bp	59
Patched1	ACCACAGGGCTATGCTCGCTCT	GGCACGGCAAACCGGACGAC	295bp	59
Pten	TCCCAGACATGACAGCCATCATCA	GCTGTGGTGGGTATGGTCTTCAA	300bp	57
Wnt3	CAGTCACACGCTCCTGCGCT	GAGCGCTACTTAGCCCGCA	419bp	59

Figure 5-2**Figure 5-2 Epidermal gene expression panel**

Genes chosen represent those whose promoters have been shown to be bound by Nanog in human and mouse systems. Many of the genes analyzed are not significantly different between the two groups, suggesting that Nanog may not be sufficient to regulate these genes in the skin. However, the expression of Jun, BMP5, FGFR2, and Jmjd1a are all drastically diminished (and statistically significant; $p < .05$) in transgenic skin.

Figure 5-3**Figure 5-3 c-Jun levels are reduced in K14.Nanog epidermis**

We assessed c-Jun protein levels by IHC after two weeks of treatment with the tumor promoter TPA. K14.Nanog skin showed lower levels of the proto-oncogene than did wild-type FVB skin (compare c to e and g). In addition, c-Jun expression is mostly exclusive with Nanog expression (serial sections f and g), even though Nanog-expressing cells are found basally and suprabasally in the IFE. In contrast, wild-type skin shows more basal c-Jun expression (denoted by black arrows in c).

Chapter 6- Ongoing Projects, Future Directions, and Significance

Ongoing-Prostate-specific Nanog expression: A constitutive model

Because much of our data concerning Nanog expression in cancer was garnered in the prostate, we wanted to specifically and robustly express Nanog in that organ. I cloned the HPCa5T-Nanog cDNA into the ARR₂Pb vector, which directs expression primarily to luminal cells in the dorsal, ventral, and lateral prostate lobes in the mouse (44). We were able to easily generate founders, and characterization of F₁ offspring revealed robust Nanog expression in the expected locales. Whole-mount H&E sections failed to reveal any hyperplastic or PIN-like lesions in mice ranging from two to six months old (Figure 6-1), but sometimes mild luminal crowding may be seen. Although this does not formally exclude Nanog expression from being sufficient to confer oncogenic phenotypes in the prostate, that possibility is reinforced by our findings in the K14.Nanog model. Additional studies to create a more favorable setting for tumorigenesis, e.g., by increasing the activity of resident stem cells through androgen-dependent regression-reconstitution cycles will be undertaken in the future to address this question. Additionally, because the probasin composite promoter is the most common means of targeting gene expression specifically to the prostate, the possibility exists to cross this mouse model with a transgenic mouse line bearing essentially any oncogene of our choosing. There also exists the possibility of crossing the K14.Nanog mouse model with the probasin-Nanog mouse to target Nanog to both the luminal and basal cell compartments simultaneously.

Summary/Significance

The significance of this work is multifaceted: First, we have generated two constitutive models that allow for the study of Nanog in a number of different tissues; similar models exist for many of the other prominent ES cell transcription factors, but this is the first Nanog transgenic model that is available to the scientific community. This model may be crossed with other models of various diseases, as we have done previously, to study a potential role for Nanog in those pathological processes. Secondly, we have demonstrated that, at least in keratin 14 cellular compartments and possibly in prostate luminal cells, Nanog overexpression is insufficient to cause tumorigenesis. It remains an open question as to whether or not Nanog can function oncogenically in the context of other malignancy-predisposing events. It seems reasonable to suspect, based on our skin tumorigenesis data, that Nanog expression at high levels may instead confer a tumor suppressive phenotype in certain tissues. Thus, like many proposed oncogenic molecules, Nanog expression may have varying effects on tumor growth, progression, and the like depending on the relevant cellular context. This dose-dependent phenotype is also very reminiscent of the role Nanog plays in ES cells. The observed phenotypes are probably highly dependent on the transcriptional program, or portion thereof, that Nanog can enact in somatic cells in the absence of some if not most of the cofactors and other transcription factors with which it is normally found in complexes in ES cells. In fibroblasts and other cells in which Nanog has been used to induce pluripotency, neither it nor any of the other transcription factors alone can reprogram somatic cells to a pluripotent state, and in ES cells low transcription factor occupancy correlates with absence of gene expression.

Future studies

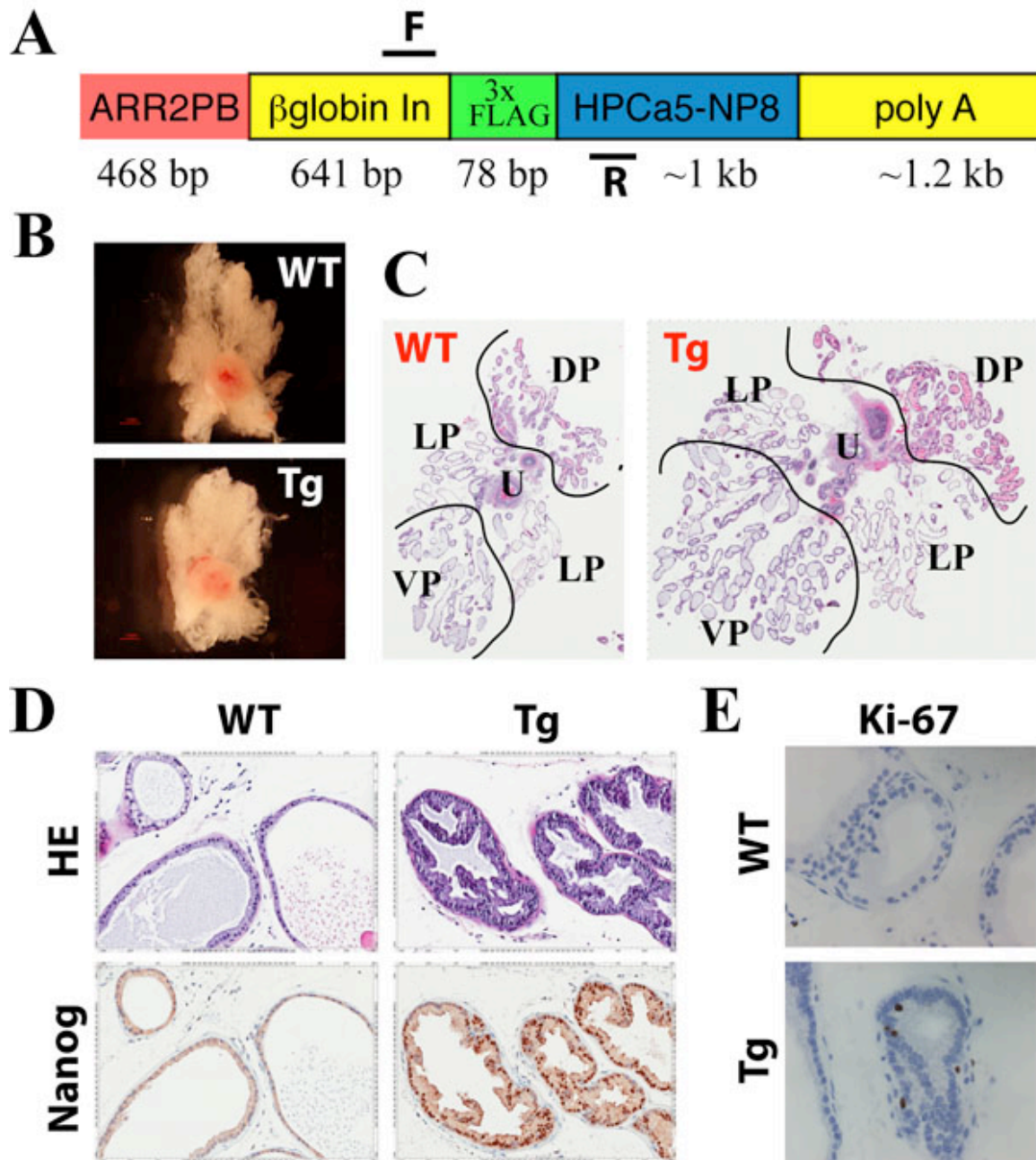
There remain a number of experiments yet to be conducted involving the K14.Nanog mouse model. The most pressing of these involves functional validation of the stem cell depletion phenomenon seen in these mice. To address this issue, *ex vivo* holoclone assays will be used as a readout of stem/progenitor cell number. If a reduction in holoclone-forming cells is observed, then we can conclude with some confidence that stem cell populations are diminished in K14.Nanog mice. Further, we will test whether addition of exogenous Bmp5 can rescue this phenotype, as has been shown by the Morris lab. If this is not the case, i.e., there is no reduction in colony-forming cells then the altered expression of stem cell markers that we observe in our transgenic mice may be seen instead simply as an abnormal display of cell surface markers.

Confirmation of our qPCR data is important also to solidify the conclusions we have drawn. To this end, Western blot of epidermal lysates for c-Jun, Bmp5, and perhaps Fgfr2 or Jmjd1a will be effected. In the case of Bmp5, this may not be feasible as it is a secreted protein, so IHC may be used as an alternative, or, failing this, the holoclone rescue experiments may suffice to validate our findings.

Future work beyond the scope of this mouse model will most likely entail moving away from a constitutive model and instead using an inducible model of Nanog expression, as any potential confounding effects owing to developmental abnormalities will be removed by selectively expressing Nanog during adulthood. Recently, we have overcome technical hurdles that precluded gain-of-function studies *in vitro*, so in order to more accurately study Nanog in prostate cancer, the original setting in which we

identified expression of this molecule, we will make prostate cancer cell lines the emphasis of future work.

Figure 6-1

**Figure 6-1 Genesis and characterization of ARR₂Pb- (Flag) Nanog Mice**

The construct used for pronuclear injections is depicted in (A). In brief, tumor-derived Nanog cDNA bearing an N-terminal Flag epitope is under the control of the androgen-responsive probasin promoter. (B-E) No significant differences exist in terms of gross morphology or in histological characterization of the glandular structures in the dorsal prostate (DP), although mild crowding of the tg lumen may be observed.

Part 2- Nanog and miR-128a

II. Nanog and miR-128a

Chapter 7- Introduction and Background

Introduction

During our intensive work concerning Nanog's role as a potential oncogene, the protein remained elusive in many cell types (ex. PC3), yet our results clearly show that reducing Nanog RNA yields a tumor-suppressive effect in these same cancer cells. This raised the possibility that the Nanog mRNA was a biologically important species, and further work suggested that it may be a molecular sink for one or more tumor-suppressive microRNA (miRNA) species. MicroRNAs are endogenous regulators of gene expression; these small nucleotides are 19-22 nucleotides in their mature form and act primarily to attenuate levels of their target mRNAs. MiRNA levels are often perturbed in cancer; tumor-suppressive microRNAs are lost or reduced and oncogenic miRNAs are amplified or otherwise increased. In this way, microRNAs behave according to classic cancer gene dogma. However, whereas many oncogenes and tumor suppressor loci have been identified, microRNAs are still something of an enigma; even though potential tumor suppressor microRNAs and oncogenic microRNAs have been identified, it is often unclear which mRNA targets are at the nexus of a given microRNA's biological effect.

We have identified a direct relationship between microRNA 128a, a tumor suppressive microRNA with known targets that are important in prostate cancer development, and the Nanog mRNA through its 3' untranslated region. We are now conducting experiments to test the biological significance of this finding.

Background

MicroRNAs (miRNAs) are small endogenous RNA species roughly 19-22 nucleotides in length that are capable of disproportionately large feats of gene expression modulation. Mature microRNAs act by binding to partially or fully complementary binding sites in the 3' untranslated region (UTR) of target messenger RNA (mRNA) species; this binding of one or more microRNAs to their respective targets destabilizes the message and leaves it susceptible to degradation. It has been speculated, and in some cases demonstrated, that a single microRNA species may have hundreds of potential targets. Conversely, each messenger RNA species may be regulated by multiple microRNAs, depending upon the length of the 3'UTR and the number of binding sites contained therein. Interestingly, it has also been reported that some microRNAs may act on the coding region of target genes, e.g., (77), although the parameters that define such interactions are less understood.

MicroRNAs were discovered quite by happenstance, and this discovery revolutionized our way of thinking about gene expression. These small RNA species represent a way to fine-tune messenger RNA levels, in some cases allowing for rapid gene expression by suppressing the mRNA until removal of the relevant microRNA. Initially, it was thought that imperfect complementarity between the microRNA seed sequence and the 3'UTR of an mRNA resulted in transcript degradation, whereas perfect complementarity was thought to elicit a mysterious translational repression that defied molecular characterization. A recent study that employed high-resolution ribosome

profiling determined that most, if not all, microRNA activity occurs through destabilization of the transcript rather than through translational repression (78).

MicroRNAs are highly conserved and possess a myriad of functions including developmental regulation, metabolism, and control of cellular proliferation (79). The intervening years since the discovery of microRNAs have taught us a great deal about their biogenesis and how this process may go awry in causing or contributing to disease. In normal miRNA genesis, primary transcripts, known as *pri*-miRNA species (which may originate from coding genes or which may be intronic in nature) are cleaved by a Drosha-containing complex to yield *pre*-miRNAs. The stem-loop-bearing *pre*-miRNA is exported to the cytoplasm where it is processed by a complex that includes Dicer along with Argonaut accessory elements. This yields the mature miRNA species that binds in a semi-complementary fashion to a plethora of mRNA targets and effects their destabilization, thereby rendering them unavailable for translation, or in rarer cases involving extensive base pairing between miR and mRNA, leads to the message's outright destruction through RISC complex-mediated cleavage. It is well-established that large-scale DNA alterations such as deletions, translocations, and the like can perturb levels of *pri*-miRNA during neoplastic transformation, but post-transcriptional miRNA regulation has also been postulated as a contributing factor in this process (80). A powerful example of this is the relationship between *let-7* and the RNA-binding protein Lin28. *Let-7* is considered the classical example of a tumor suppressive microRNA, as it possesses high affinity for oncogenes such as *Ras*, *Hmga2*, and *Caspase 3* (81-83) and is diminished in lung cancer (84). Lin 28 acts to sequester *let-7* and other microRNA species, which allows terminal uridyl transferases (TUTs) to

associate with the RNA-protein complex and tag the pre-microRNA species for degradation by adding multiple uridyl residues to the 3' end of the miRNA (85, 86).

MicroRNAs and non-coding RNA species

Recently, it has become apparent that pseudogenes may regulate microRNA activity. Pseudogenes are molecular fossils, incomplete or otherwise non-functional, i.e., non-protein-coding genes born of the parental locus and inserted back into the genome in a different location (usually through a retrotransposition event). In the rare case that such a doppelganger gene retains the ability to encode a functional protein, it is instead designated a retrogene. Genes that are expressed embryonically are more likely to possess pseudogenes, as transposons may be active in the relatively accessible chromatin configuration present during this window of development. In fact, Oct-4 has upwards of 13 pseudogenes, while Nanog has 10 pseudogenes and one retrogene. These pseudogenes may be of two forms, processed or unprocessed, each reflecting a different origin. Processed pseudogenes are derived from expressed mRNA that undergoes retrotransposition and is inserted into the genome, and therefore these species lack introns and promoters of their own. Non-processed pseudogenes arise from duplication of the parental gene; over time and in the absence of selective pressure these duplicates acquire mutations, deletions, and the like that render them non-functional.

Because of their similarity to transcripts encoding functional gene products, pseudogenes are oftentimes confused for their parental transcripts, and as such experimental design (including choice of primers) and interpretation must be undertaken carefully. A report in 2007, issued amidst a flurry of stem cell research, cited numerous

other studies as derelict in considering Oct-4 pseudogenes in their work, and concluded that significant confusion had been created in the scientific community as a result (87) .

The molecular resemblance of a pseudogene to a parental gene of origin serves as more than an experimental irritant, however. As pseudogene transcripts “look” like *bona fide* protein-coding gene mRNAs, they may serve as decoys for the various mechanisms that regulate mRNA transcripts, including microRNAs. In instances where the transcript has retained relevant 3'UTR or coding region miRNA binding sites, the microRNA may bind to the “artificial” transcript instead of the authentic one; in this way, miRNA activity is diverted away from a particular gene. This phenomenon was demonstrated convincingly using PTEN and its decoy pseudogene PTENP1 as archetypes, as targeting of PTENP1 results in an increase in microRNA-mediated PTEN loss (88). This ability of pseudogenes to sponge or subvert miRNA activity represents yet another layer of regulation of microRNAs, as the mature form must navigate a sea of potential binding partners in order to exert its influence on a “true” target.

MicroRNA 128a- a candidate tumor suppressor

Among the class of tumor suppressive microRNAs, miR-128a represents a largely uninvestigated miR that may be highly relevant to the development and progression of prostate cancer. It is among a handful of microRNAs that is significantly expressed in the neuronal lineage: It is largely absent from neural stem cells (89) but is highly expressed in mature, terminally-differentiated neurons (90). A number of recent studies lend credence to the notion of miR-128a as a tumor suppressor in glioma, including those that identified Bmi1 and E2F3 (91, 92), two proteins whose

overexpression is known to contribute to tumorigenesis, as potential targets. Evidence of miR-128a's role in suppression of prostate cancer comes in the form of a proteomics-based study in which miR-128a targets were found to be expressed at higher levels in prostate adenocarcinomas than in benign prostatic tissue (93); indeed, metastatic PCa showed even higher levels of these proteins than in situ disease, suggesting that miR-128a is progressively diminished during progression of the disease. Loss of miR-128a was shown to result in increased invasion and migration of prostate cancer cells *in vitro*. Even more promising was the finding that miR-128a levels are consistently lower in primary prostate cancer samples than in benign tissue (94). The great unknown in this equation is how miR-128a levels are diminished in prostate cancer. To date, no mechanism of miR-128a loss has been reported, yet all of the usual suspects are possible, including but not limited to promoter methylation/chromatin silencing, genetic deletion, and the tantalizing possibility that decoy mRNA transcripts are increasingly expressed as cells become malignant.

A promising but unelaborated-upon finding in this work is the close relationship between the Polycomb1 complex protein expression signature and that of microRNA 128a. This greatly augments the connection between miR-128a and Bmi1 in prostate cancer and suggests an inverse relationship between the two. Bmi1 normally functions by associating with RING1B, PH1, and CBX4 in the Polycomb1 complex; this cluster of proteins is responsible for reading the H3K27 repressive chromatin mark laid down by the Polycomb 2 complex, which is composed of an EZH2 enzyme, as well as EED, SUZ12, and RBPA48 accessory proteins. Bmi1/Polycomb1 complex silencing is thought to be dependent on the complex's ability to add ubiquitin to H2A, which may

result in RNA polymerase pausing or cessation of transcription (95). It is well-established that Bmi1 is overexpressed in many instances of prostate adenocarcinoma, and it has been recently evinced as an important mediator of self-renewal in normal and malignant prostatic stem-like cells (96).

Chapter 8- Materials and Methods

Cell culture

LNCaP, PC3, and DU145 cells were cultured in RPMI media (Invitrogen) supplemented with 8% fetal bovine serum (FBS). RWPE-1 cells were cultured in KBM-Gold medium (Lonza) supplemented with additional growth factors. All cell culture was performed in antibiotic-free conditions.

Clonal and clonogenic assays

Clonal assays were conducted by plating 100 or 200 cells per well of a six-well dish following experimental manipulation. Cells were allowed to attach for 24-48 hours before the media was changed. Colonies were scored and photographed two weeks later. Clonogenic assays were performed identically but cells were plated on low-attachment tissue culture dishes. Spheres were counted and photographed two weeks post-plating.

Luciferase assays

The Nanog 3' UTR was cloned into the MCS of pMirREPORT (Ambion); a renilla luciferase-coding plasmid was used as an internal control. Cells were seeded 40k per well of a 24-well dish and allowed to attach for 24 hours prior to transfection. Mir-128a and a non-targeting control (Ambion) were transfected into target cells at a final concentration of 32nM using either Lipofectamine 2000 or RNAiMAX (Invitrogen/Life Technologies) reagents per the manufacturer's protocol. 48 hours after transfection, the Dual Luciferase assay kit (Promega) was used to induce chemiluminescence, which was detected and measured on a Gen-Probe chemiluminometer.

Site-directed mutagenesis

The 9-mer seed sequence of the miR-128a binding site in the Nanog 3'UTR was mutated from 5' TTCACTGTG to 5' TTCGAGTTG using the Stratagene QuikChange kit as per manufacturer's instructions.

RNA extraction and quantification of Mir-128a

Total RNA was extracted from cultured cells using the Mirvana PARIS kit (Ambion). Briefly, cells were lysed in a mild buffer and RNAses were inactivated with subsequent addition of a GITC-containing buffer. Acid phenol-chloroform was added, and the aqueous phase was harvested following centrifugation. This was mixed with 1.25x volumes of ethanol and applied to a glass-silica column, centrifuged, washed, and eluted with nuclease-free water. RNA integrity was analyzed on the Agilent Bioanalyzer nanochip. MicroRNA was reverse transcribed using the Taqman MicroRNA reverse transcription kit, and microRNA levels were determined using the Taqman Small RNA assay (Applied Biosystems). Sample measurements were averaged and means were compared using the Student's t test.

Nanog knockdown via siRNA

Prostate cancer cells were plated and allowed to reach three-fourths confluence prior to transfection with siNanog SMARTPOOL siRNA or non-targeting SMARTPOOL siRNA (Dharmacon) using RNAiMAX transfection reagent (Invitrogen).

Nanog knockdown via lentiviral-mediated short hairpin RNA

Lentivirus bearing a short-hairpin RNA directed against Nanog or bearing no shRNA (empty vector) was generated as previously described (36). Cells that expressed the short hairpin or empty vector were selected by sorting for GFP⁺ cells using a BD Aria flow cytometer.

Chapter 9- Examining the Nanog/miR-128a axis

Nanog regulation by mir-128a

Our previous work showed that diminution of Nanog RNA levels had a drastic impact on prostate cancer development (36). However, our transgenic models of Nanog overexpression, both keratin 14- and ARR₂Pb-driven, failed to show any neoplastic or even pre-neoplastic alterations. Additionally, the protein has remained elusive- as assessed by Western blot, mass spectrometry, immunoprecipitation, etc...- in various primary and cultured cancer cells such as PC3, although the prostate cancer cell line DU145 numbers among those cell lines where the protein is scant yet present. A compelling study from the Orkin lab demonstrated that the so-called “ES cell gene expression signatures” thought to be evident in somatic cancers were in fact largely a reflection of the transcriptional program carried out by Myc (97), a well-known oncogene and transcription factor that is expressed at high levels in many cancer types. We therefore could not exclude the possibility that the biologically-relevant species in a cancerous context is the RNA rather than the protein. With the introduction of a “ceRNA” hypothesis by the Pandolfi lab (98), one in which RNA species regulate one another by competing for microRNA binding, we wondered if this model may apply to our Nanog loss-of-function observations. Our animal models and subsequent *in vitro* gain-of-function experiments failed to account for a potential role of the Nanog 3’UTR, as our cloned Nanog cDNA lacks the 3’UTR that is instrumental in microRNA regulation.

In order for Nanog to fit this paradigm, it should be capable of acting as a molecular sink to siphon off potential tumor suppressive microRNAs from their *bona*

fide targets. We therefore conducted a thorough search of the various microRNA/ miR target databases and combined this approach with an exhaustive literature search in order to determine if the Nanog 3'UTR contained any binding sites for tumor suppressor microRNAs. Two independent microRNA target prediction algorithms, MicroCosm V5 and miRanda, indicate a strong binding site for mir-128a in the Nanog 3'UTR (Fig 9-1A). In fact, this is the only microRNA binding site in the 3'UTR that is predicted by *both* computational programs.

In order to test whether or not this predicted binding could occur biologically, I utilized the pMIR-REPORT vector into which the Nanog 3'UTR had been cloned upstream of the firefly luciferase coding sequence. Addition of mir-128a, but not non-targeting microRNA, resulted in greatly diminished luciferase output (Fig 9-1B and C). Mutation of the seed sequence entirely abolished miR-128a regulation of Nanog 3'UTR-dependent firefly luciferase activity. This suggests that the Nanog 3'UTR is a *bona fide* target of miR-128a.

To further this point, I wanted to determine if depletion of endogenous Nanog mRNA could liberate miR-128a. I predicted that removing Nanog RNA via siRNA knockdown would result in a net increase in the levels of miR-128a, and I therefore transfected PC3 and LNCaP cells with siRNA (directed against Nanog or noncoding) and assayed microRNA-128a levels 48 hours later. I found that miR-128a levels consistently increased by about 16-17% in those cells that were robbed of Nanog mRNA (Fig 9-2), suggesting that Nanog mRNA is a potent reservoir for miR-128a. To extend this finding to situations in which Nanog is chronically absent, I introduced a GFP-expressing lentivirus bearing a short hairpin RNA directed against Nanog (or an empty

vector) into PC3 cells and sorted for GFP-positive cells. Cells in which Nanog was diminished expressed roughly 40% more miR-128a than cells that were infected with only the empty vector.

Mir-128a as a tumor suppressor in PCa

Next, I opted to test whether miR-128a, which has been reported to inhibit growth of glioma cells, can function as a tumor suppressor in prostate cancer cells as well. To this end, I transfected miR-128a or non-targeting microRNA control into LNCaP cells and assayed for clonal growth. After two weeks, only one-third the number of cells transfected with mir-128a as compared to those transfected with a non-targeting species had established holoclones (Fig 9-3A). Primary clonogenic assays, which measure both a cell's ability to grow in anchorage-independent conditions and its proliferative capacity, revealed no difference between the two groups. However, secondary clonogenic assays, a better representation of the stem cell-like property of self-renewal, showed that fewer mir-128a-transfected cells could form spheres than could non-coding miRNA-transfected cells (Fig 9-3B and C).

Figure 9-1

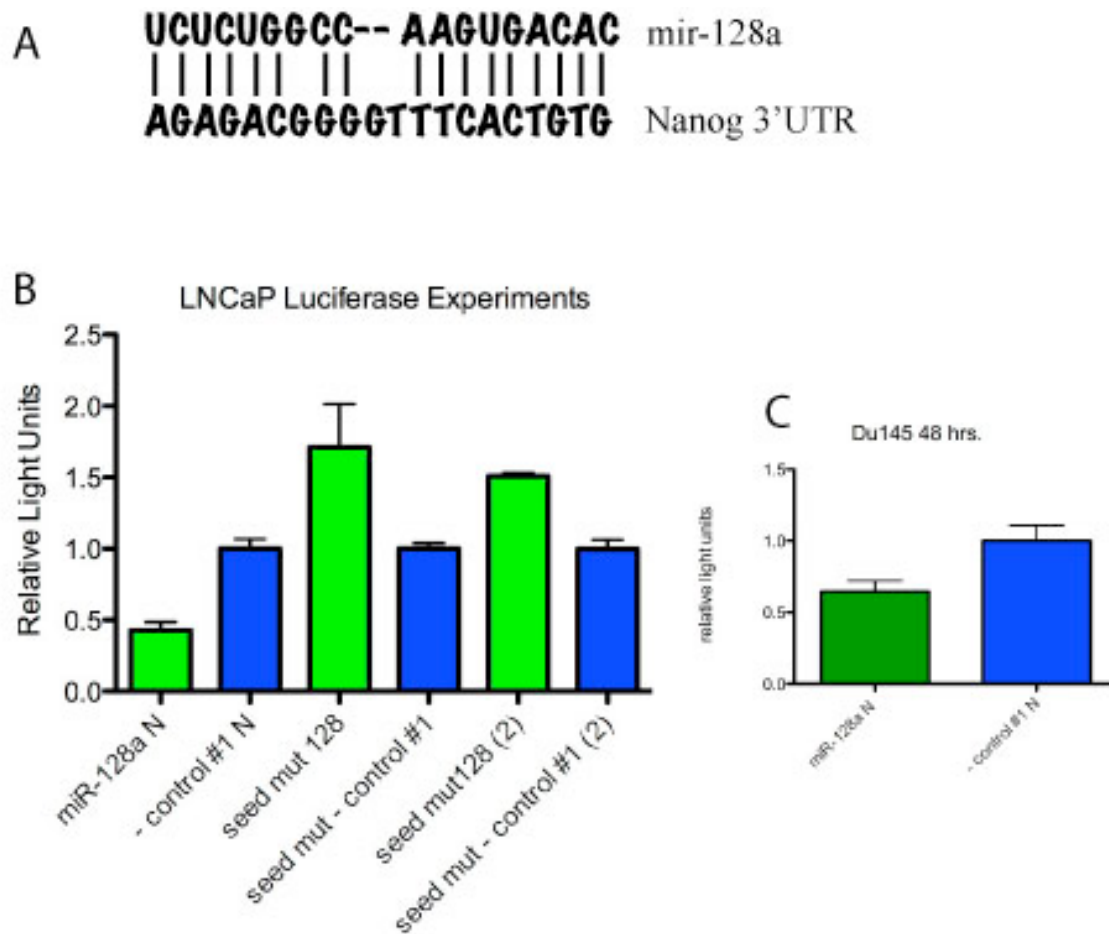
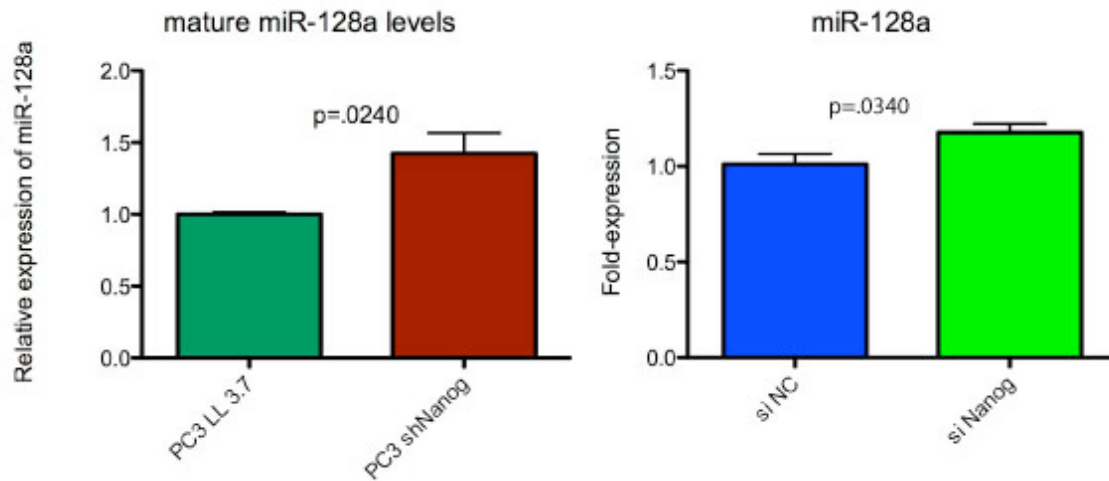
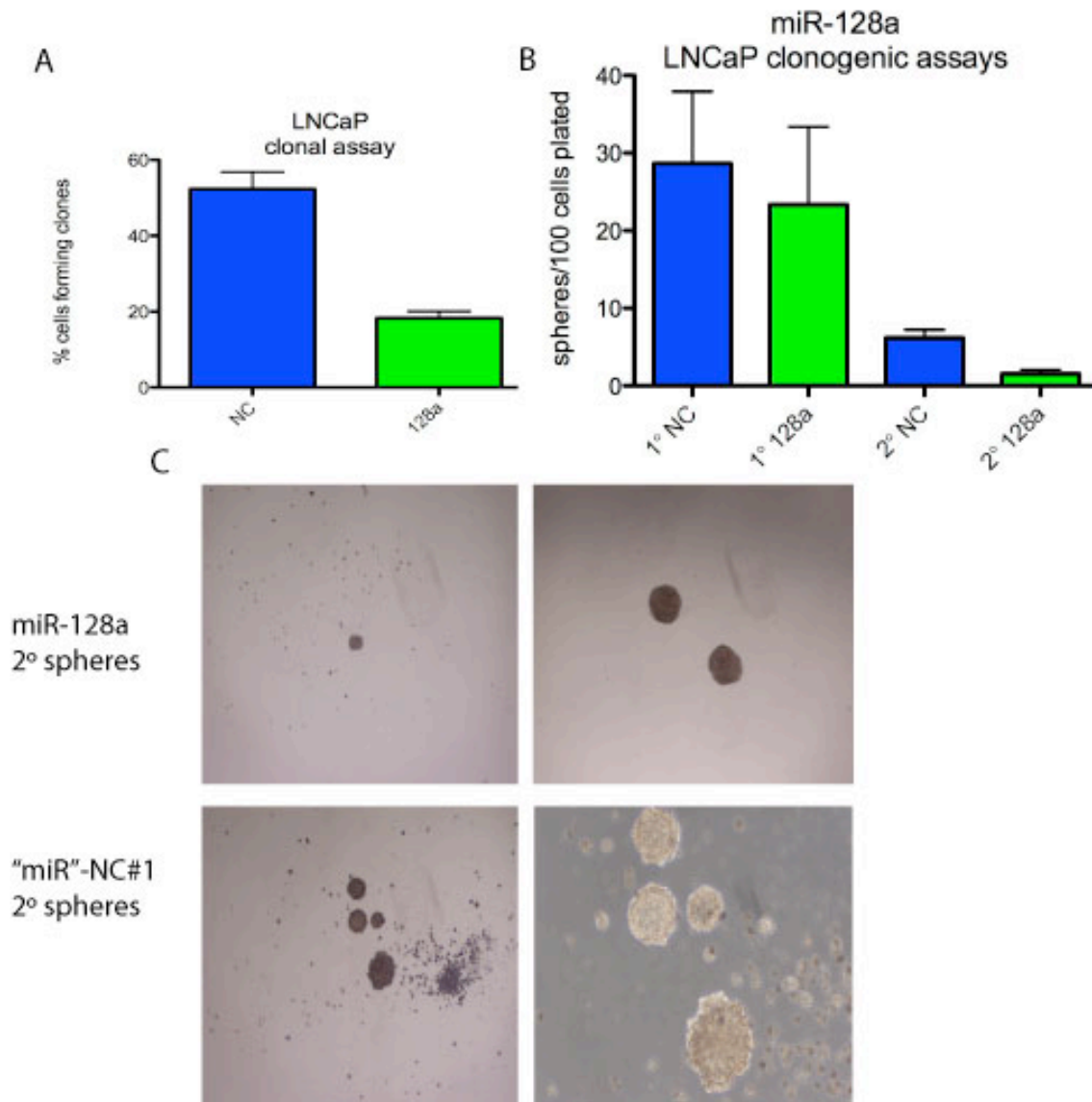


Figure 9-1 Mir-128a can regulate the Nanog 3'UTR The nucleotide alignment of mir-128a's mature form and the relevant predicted binding site in the Nanog 3'UTR suggest a strong interaction (A). Luciferase experiments confirm the strength of the interaction, as the presence of this binding site alone is sufficient to confer a 60 percent reduction in luciferase output when exogenous miR-128a is added (B); this phenomenon can be observed in DU145 cells as well (C). Mutation of four nucleotides in the seed region renders miR-128a unable to act on the Nanog 3'UTR (B); interestingly, firefly luciferase activity soars well past the baseline.

Figure 9-2**Figure 9-2 Reduction of endogenous Nanog levels leads to an increase in miR-128a levels**

I employed two different strategies to determine if loss of one potential target mRNA species would result in an increase in mature, “free” miR-128a. First, I employed a long-term, stable knockdown of Nanog by infecting PC3 cells with a lentivirus that expresses a short hairpin RNA targeting Nanog. When compared to an empty vector control, cells in which Nanog has been targeted show a 40-percent increase in miR-128a levels.

The second strategy uses siRNA for short-term analyses: Cancer cell lines (including PC3 and LNCaP) in which Nanog levels have been diminished show an approximate 17 percent rise in miR-128a 48 hours after transfection with siRNA.

Figure 9-3**Figure 9-3 Mir-128a impacts PCa cell line clonal and clonogenic growth**

LNCaP cells transfected with miR-128a display one-third of the number of holoclones relative to controls after two weeks (A). Primary clonogenic assays, which measure anchorage-independent growth and proliferative potential, showed no difference between cells transfected with miR-128a and those transfected with a non-targeting artificial microRNA (B). However, secondary clonogenic assays confirm that sphere-forming ability is progressively lost when exogenous mir-128a is added (B and C).

Nanog mRNA miR-ly as a sponge?

It is likely though unproven that a given mRNA message may bind more than one microRNA species at a time if the relevant binding sites are unoccupied, and that this binding is dynamic and constantly in a state of equilibrium. If this is the case, then it is also likely that the sum total of a particular RNA message's impact on the microRNA pool is determined by the number of miRNA binding sites and the affinity of those binding sites for their respective microRNAs. It is therefore likely that Nanog's 3'UTR does not only contribute to tumorigenesis by acting on miR-128a, but may act on other species in parallel or even simultaneously. One promising target is mir-34a, a tumor suppressive microRNA that our lab identified as a potent regulator of cancer stem cells through CD44. We conducted preliminary studies into the possible connection between mir-34a and Nanog, but although luciferase assays showed regulation of the Nanog 3'UTR by mir-34a, the activity was weak and we therefore decided not to pursue that avenue of research any further. However, a recent paper has confirmed this regulation in demonstrating that mir-34a impedes reprogramming of somatic cell (99), and thus it seems likely that the Nanog 3'UTR may be able to act as a sponge for this important tumor suppressor as well.

Conversely, it is highly probable that Nanog mRNA is not the sole RNA decoy for miR-128a (or miR-34a, for that matter). As this concept is in its nascency, a systematic study of pseudogenes and other likely RNA sponges (e.g. long intergenic noncoding or linc RNAs) that are expressed in somatic cancers has not been conducted. It is likely also that protein-coding genes may be activated in order to siphon off

microRNAs, provided that those genes' protein products do not impose undue proliferative or other competitive constraints on the cancer cell.

Chapter 10- Significance and Future Directions

Future Studies

I am currently in the process of conducting *in vivo* xenograft experiments in order to verify miR-128a's potential as a tumor suppressor in prostate cancer. In addition, I will attempt to determine if expressing the Nanog 3'UTR alone can enhance tumorigenesis. As it is believed that Bmi1 is one of the most important targets for miR-128a in the prostate, and perhaps *the* most important of its targets during development of prostate cancer, I will conduct immunoprecipitation of Argonaut proteins and perform real-time PCR in both Nanog-depleted and control samples. This would be the most powerful method of showing that the Nanog transcript is shielding Bmi1 from microRNA activity; it would also allow for the effect of other potentially shared microRNAs to be observed.

Additionally, it will be important to test how Nanog mRNA functions as a ceRNA in its native setting, that is, in ES or even embryonal carcinoma cells. In this setting, the mRNA is much more abundantly expressed, and the protein is abundant as well, so this may well represent an instance of a protein-coding mRNA species acting to regulate other mRNA species. This would not be unsurprising given the complexity inherent in establishing and maintaining the pluripotent state in the blastocyst and its *in vitro* derivative. This system can also be employed in order to test whether miR-128a activity can, as expected, decrease the level of the Nanog protein.

Exciting, large-scale studies aimed at identifying the range of ceRNAs which Nanog mRNA may compete with for microRNA binding are beyond the scope of this

lab's expertise, but fully elucidating these competitors will allow for a better appreciation of the biological role of Nanog mRNA in the setting of tumorigenesis.

Significance

It is important to determine in which cancers or even in which individual tumors Nanog is expressed solely at the level of RNA, as we cannot rule out oncogenic activity of the protein, although the latter seems mostly confined to germ cell tumors. This may be because of the ironclad nature of the silencing that ES-cell/pluripotency genes seem to undergo as they transition to somatic cells. In essence, any latent contribution to tumor growth is strictly hypothetical as the parental genes are unable to undergo reactivation. The form of Nanog that we detect in cancer cells originates from the NanogP8 locus, which lacks a promoter of its own; expression from this region of the genome is therefore very minimal. This may explain why the protein is essentially undetectable in many cancer cell types, as the mRNA must overcome a variety of obstacles including microRNA-induced instability and exosome activity before ever encountering a ribosome. If further work determines that Nanog mRNA is the important biological species in somatic tumors, this will ameliorate cancer research by de-emphasizing work on the Nanog protein as a potential effector of tumorigenesis and instead will highlight the appropriate miRs, including miR-128a, and their respective authentic, protein-coding targets. A final possibility is that in circumstances where the protein is evident, the Nanog mRNA and protein each may be oncogenic entities and that their combined actions may collaborate to effect tumor development through different mechanisms.

References

1. Shackleton, M., E. Quintana, E. R. Fearon, and S. J. Morrison. 2009. Heterogeneity in cancer: cancer stem cells versus clonal evolution. *Cell* 138:822-829.
2. Visvader, J. E., and G. J. Lindeman. 2008. Cancer stem cells in solid tumours: accumulating evidence and unresolved questions. *Nat Rev Cancer* 8:755-768.
3. Bonnet, D., and J. E. Dick. 1997. Human acute myeloid leukemia is organized as a hierarchy that originates from a primitive hematopoietic cell. *Nat Med* 3:730-737.
4. Lapidot, T., C. Sirard, J. Vormoor, B. Murdoch, T. Hoang, J. Caceres-Cortes, M. Minden, B. Paterson, M. A. Caligiuri, and J. E. Dick. 1994. A cell initiating human acute myeloid leukaemia after transplantation into SCID mice. *Nature* 367:645-648.
5. Al-Hajj, M., M. S. Wicha, A. Benito-Hernandez, S. J. Morrison, and M. F. Clarke. 2003. Prospective identification of tumorigenic breast cancer cells. *Proc Natl Acad Sci U S A* 100:3983-3988.
6. Patrawala, L., T. Calhoun, R. Schneider-Broussard, H. Li, B. Bhatia, S. Tang, J. G. Reilly, D. Chandra, J. Zhou, K. Claypool, L. Coghlan, and D. G. Tang. 2006. Highly purified CD44⁺ prostate cancer cells from xenograft human tumors are enriched in tumorigenic and metastatic progenitor cells. *Oncogene* 25:1696-1708.
7. Hassan, K. A., G. Chen, G. P. Kalemkerian, M. S. Wicha, and D. G. Beer. 2009. An embryonic stem cell-like signature identifies poorly differentiated lung

- adenocarcinoma but not squamous cell carcinoma. *Clin Cancer Res* 15:6386-6390.
8. Ben-Porath, I., M. W. Thomson, V. J. Carey, R. Ge, G. W. Bell, A. Regev, and R. A. Weinberg. 2008. An embryonic stem cell-like gene expression signature in poorly differentiated aggressive human tumors. *Nat Genet* 40:499-507.
 9. Wong, D. J., H. Liu, T. W. Ridky, D. Cassarino, E. Segal, and H. Y. Chang. 2008. Module map of stem cell genes guides creation of epithelial cancer stem cells. *Cell Stem Cell* 2:333-344.
 10. Widschwendter, M., H. Fiegl, D. Egle, E. Mueller-Holzner, G. Spizzo, C. Marth, D. J. Weisenberger, M. Campan, J. Young, I. Jacobs, and P. W. Laird. 2007. Epigenetic stem cell signature in cancer. *Nat Genet* 39:157-158.
 11. Ohm, J. E., K. M. McGarvey, X. Yu, L. Cheng, K. E. Schuebel, L. Cope, H. P. Mohammad, W. Chen, V. C. Daniel, W. Yu, D. M. Berman, T. Jenuwein, K. Pruitt, S. J. Sharkis, D. N. Watkins, J. G. Herman, and S. B. Baylin. 2007. A stem cell-like chromatin pattern may predispose tumor suppressor genes to DNA hypermethylation and heritable silencing. *Nat Genet* 39:237-242.
 12. Wang, J., S. Rao, J. Chu, X. Shen, D. N. Levasseur, T. W. Theunissen, and S. H. Orkin. 2006. A protein interaction network for pluripotency of embryonic stem cells. *Nature* 444:364-368.
 13. Kim, J., J. Chu, X. Shen, J. Wang, and S. H. Orkin. 2008. An extended transcriptional network for pluripotency of embryonic stem cells. *Cell* 132:1049-1061.

14. Boyer, L. A., T. I. Lee, M. F. Cole, S. E. Johnstone, S. S. Levine, J. P. Zucker, M. G. Guenther, R. M. Kumar, H. L. Murray, R. G. Jenner, D. K. Gifford, D. A. Melton, R. Jaenisch, and R. A. Young. 2005. Core transcriptional regulatory circuitry in human embryonic stem cells. *Cell* 122:947-956.
15. Zbinden, M., A. Duquet, A. Lorente-Trigos, S. N. Ngwabyt, I. Borges, and A. Ruiz i Altaba. 2010. NANOG regulates glioma stem cells and is essential in vivo acting in a cross-functional network with GLI1 and p53. *EMBO J* 29:2659-2674.
16. Chiou, S. H., M. L. Wang, Y. T. Chou, C. J. Chen, C. F. Hong, W. J. Hsieh, H. T. Chang, Y. S. Chen, T. W. Lin, H. S. Hsu, and C. W. Wu. 2010. Coexpression of Oct4 and Nanog enhances malignancy in lung adenocarcinoma by inducing cancer stem cell-like properties and epithelial-mesenchymal transdifferentiation. *Cancer Res* 70:10433-10444.
17. Yori, J. L., D. D. Seachrist, E. Johnson, K. L. Lozada, F. W. Abdul-Karim, L. A. Chodosh, W. P. Schiemann, and R. A. Keri. Kruppel-like factor 4 inhibits tumorigenic progression and metastasis in a mouse model of breast cancer. *Neoplasia* 13:601-610.
18. Foster, K. W., Z. Liu, C. D. Nail, X. Li, T. J. Fitzgerald, S. K. Bailey, A. R. Frost, I. D. Louro, T. M. Townes, A. J. Paterson, J. E. Kudlow, S. M. Lobo-Ruppert, and J. M. Ruppert. 2005. Induction of KLF4 in basal keratinocytes blocks the proliferation-differentiation switch and initiates squamous epithelial dysplasia. *Oncogene* 24:1491-1500.
19. Yori, J. L., D. D. Seachrist, E. Johnson, K. L. Lozada, F. W. Abdul-Karim, L. A. Chodosh, W. P. Schiemann, and R. A. Keri. 2011. Kruppel-like factor 4 inhibits

- tumorigenic progression and metastasis in a mouse model of breast cancer. *Neoplasia* 13:601-610.
20. Hochedlinger, K., Y. Yamada, C. Beard, and R. Jaenisch. 2005. Ectopic expression of Oct-4 blocks progenitor-cell differentiation and causes dysplasia in epithelial tissues. *Cell* 121:465-477.
 21. Liang, J., M. Wan, Y. Zhang, P. Gu, H. Xin, S. Y. Jung, J. Qin, J. Wong, A. J. Cooney, D. Liu, and Z. Songyang. 2008. Nanog and Oct4 associate with unique transcriptional repression complexes in embryonic stem cells. *Nat Cell Biol* 10:731-739.
 22. Pan, G. J., and D. Q. Pei. 2003. Identification of two distinct transactivation domains in the pluripotency sustaining factor nanog. *Cell Res* 13:499-502.
 23. Pan, G., and D. Pei. 2005. The stem cell pluripotency factor NANOG activates transcription with two unusually potent subdomains at its C terminus. *J Biol Chem* 280:1401-1407.
 24. Oh, J. H., H. J. Do, H. M. Yang, S. Y. Moon, K. Y. Cha, H. M. Chung, and J. H. Kim. 2005. Identification of a putative transactivation domain in human Nanog. *Exp Mol Med* 37:250-254.
 25. Mullin, N. P., A. Yates, A. J. Rowe, B. Nijmeijer, D. Colby, P. N. Barlow, M. D. Walkinshaw, and I. Chambers. 2008. The pluripotency rheostat Nanog functions as a dimer. *Biochem J* 411:227-231.
 26. Chambers, I., D. Colby, M. Robertson, J. Nichols, S. Lee, S. Tweedie, and A. Smith. 2003. Functional expression cloning of Nanog, a pluripotency sustaining factor in embryonic stem cells. *Cell* 113:643-655.

27. Mitsui, K., Y. Tokuzawa, H. Itoh, K. Segawa, M. Murakami, K. Takahashi, M. Maruyama, M. Maeda, and S. Yamanaka. 2003. The homeoprotein Nanog is required for maintenance of pluripotency in mouse epiblast and ES cells. *Cell* 113:631-642.
28. Chambers, I., J. Silva, D. Colby, J. Nichols, B. Nijmeijer, M. Robertson, J. Vrana, K. Jones, L. Grotewold, and A. Smith. 2007. Nanog safeguards pluripotency and mediates germline development. *Nature* 450:1230-1234.
29. Takahashi, K., and S. Yamanaka. 2006. Induction of pluripotent stem cells from mouse embryonic and adult fibroblast cultures by defined factors. *Cell* 126:663-676.
30. Silva, J., J. Nichols, T. W. Theunissen, G. Guo, A. L. van Oosten, O. Barrandon, J. Wray, S. Yamanaka, I. Chambers, and A. Smith. 2009. Nanog is the gateway to the pluripotent ground state. *Cell* 138:722-737.
31. Alldridge, L., G. Metodiev, C. Greenwood, K. Al-Janabi, L. Thwaites, P. Sauven, and M. Metodiev. 2008. Proteome profiling of breast tumors by gel electrophoresis and nanoscale electrospray ionization mass spectrometry. *J Proteome Res* 7:1458-1469.
32. Zbinden, M., A. Duquet, A. Lorente-Trigos, S. N. Ngwabyt, I. Borges, and A. Ruiz i Altaba. NANOG regulates glioma stem cells and is essential in vivo acting in a cross-functional network with GLI1 and p53. *EMBO J* 29:2659-2674.
33. Bourguignon, L. Y., K. Peyrollier, W. Xia, and E. Gilad. 2008. Hyaluronan-CD44 interaction activates stem cell marker Nanog, Stat-3-mediated MDR1 gene

- expression, and ankyrin-regulated multidrug efflux in breast and ovarian tumor cells. *J Biol Chem* 283:17635-17651.
34. Zhang, J., X. Wang, M. Li, J. Han, B. Chen, B. Wang, and J. Dai. 2006. NANOGP8 is a retrogene expressed in cancers. *FEBS J* 273:1723-1730.
 35. Meng, H. M., P. Zheng, X. Y. Wang, C. Liu, H. M. Sui, S. J. Wu, J. Zhou, Y. Q. Ding, and J. M. Li. Overexpression of nanog predicts tumor progression and poor prognosis in colorectal cancer. *Cancer Biol Ther* 9.
 36. Bussolati, B., S. Bruno, C. Grange, U. Ferrando, and G. Camussi. 2008. Identification of a tumor-initiating stem cell population in human renal carcinomas. *FASEB J* 22:3696-3705.
 37. Zhang, S., C. Balch, M. W. Chan, H. C. Lai, D. Matei, J. M. Schilder, P. S. Yan, T. H. Huang, and K. P. Nephew. 2008. Identification and characterization of ovarian cancer-initiating cells from primary human tumors. *Cancer Res* 68:4311-4320.
 38. Jeter, C. R., M. Badeaux, G. Choy, D. Chandra, L. Patrawala, C. Liu, T. Calhoun-Davis, H. Zaehres, G. Q. Daley, and D. G. Tang. 2009. Functional evidence that the self-renewal gene NANOG regulates human tumor development. *Stem Cells* 27:993-1005.
 39. Tumber, T., G. Guasch, V. Greco, C. Blanpain, W. E. Lowry, M. Rendl, and E. Fuchs. 2004. Defining the epithelial stem cell niche in skin. *Science* 303:359-363.

40. Byrne, C., and E. Fuchs. 1993. Probing keratinocyte and differentiation specificity of the human K5 promoter in vitro and in transgenic mice. *Mol Cell Biol* 13:3176-3190.
41. Sawicki, J. A., and C. J. Rothman. 2002. Evidence for stem cells in cultures of mouse prostate epithelial cells. *Prostate* 50:46-53.
42. Bocker, W., R. Moll, C. Poremba, R. Holland, P. J. Van Diest, P. Dervan, H. Burger, D. Wai, R. Ina Diallo, B. Brandt, H. Herbst, A. Schmidt, M. M. Lerch, and I. B. Buchwallow. 2002. Common adult stem cells in the human breast give rise to glandular and myoepithelial cell lineages: a new cell biological concept. *Lab Invest* 82:737-746.
43. Kasper, S., P. S. Rennie, N. Bruchovsky, L. Lin, H. Cheng, R. Snoek, K. Dahlman-Wright, J. A. Gustafsson, R. P. Shiu, P. C. Sheppard, and R. J. Matusik. 1999. Selective activation of the probasin androgen-responsive region by steroid hormones. *J Mol Endocrinol* 22:313-325.
44. Zhang, J., T. Z. Thomas, S. Kasper, and R. J. Matusik. 2000. A small composite probasin promoter confers high levels of prostate-specific gene expression through regulation by androgens and glucocorticoids in vitro and in vivo. *Endocrinology* 141:4698-4710.
45. Potten, C. S. 1974. The epidermal proliferative unit: the possible role of the central basal cell. *Cell Tissue Kinet* 7:77-88.
46. Bickenbach, J. R. 1981. Identification and behavior of label-retaining cells in oral mucosa and skin. *J Dent Res* 60 Spec No C:1611-1620.

47. Barrandon, Y., and H. Green. 1987. Three clonal types of keratinocyte with different capacities for multiplication. *Proc Natl Acad Sci U S A* 84:2302-2306.
48. Jaks, V., N. Barker, M. Kasper, J. H. van Es, H. J. Snippert, H. Clevers, and R. Toftgard. 2008. Lgr5 marks cycling, yet long-lived, hair follicle stem cells. *Nat Genet* 40:1291-1299.
49. Nilsson, J., C. Vallbo, D. Guo, I. Golovleva, B. Hallberg, R. Henriksson, and H. Hedman. 2001. Cloning, characterization, and expression of human LIG1. *Biochem Biophys Res Commun* 284:1155-1161.
50. Gur, G., C. Rubin, M. Katz, I. Amit, A. Citri, J. Nilsson, N. Amariglio, R. Henriksson, G. Rechavi, H. Hedman, R. Wides, and Y. Yarden. 2004. LRIG1 restricts growth factor signaling by enhancing receptor ubiquitylation and degradation. *EMBO J* 23:3270-3281.
51. Jensen, K. B., C. A. Collins, E. Nascimento, D. W. Tan, M. Frye, S. Itami, and F. M. Watt. 2009. Lrig1 expression defines a distinct multipotent stem cell population in mammalian epidermis. *Cell Stem Cell* 4:427-439.
52. Snippert, H. J., A. Haegebarth, M. Kasper, V. Jaks, J. H. van Es, N. Barker, M. van de Wetering, M. van den Born, H. Begthel, R. G. Vries, D. E. Stange, R. Toftgard, and H. Clevers. 2010. Lgr6 marks stem cells in the hair follicle that generate all cell lineages of the skin. *Science* 327:1385-1389.
53. Nijhof, J. G., K. M. Braun, A. Giangreco, C. van Pelt, H. Kawamoto, R. L. Boyd, R. Willemze, L. H. Mullenders, F. M. Watt, F. R. de Gruijl, and W. van Ewijk. 2006. The cell-surface marker MTS24 identifies a novel population of follicular

- keratinocytes with characteristics of progenitor cells. *Development* 133:3027-3037.
54. Kangsamaksin, T., H. J. Park, C. S. Trempus, and R. J. Morris. 2007. A perspective on murine keratinocyte stem cells as targets of chemically induced skin cancer. *Mol Carcinog* 46:579-584.
 55. Morris, R. J., K. A. Tryson, and K. Q. Wu. 2000. Evidence that the epidermal targets of carcinogen action are found in the interfollicular epidermis of infundibulum as well as in the hair follicles. *Cancer Res* 60:226-229.
 56. Lu, J., O. Rho, E. Wilker, L. Beltran, and J. Digiovanni. 2007. Activation of epidermal akt by diverse mouse skin tumor promoters. *Mol Cancer Res* 5:1342-1352.
 57. Abel, E. L., J. M. Angel, K. Kiguchi, and J. DiGiovanni. 2009. Multi-stage chemical carcinogenesis in mouse skin: fundamentals and applications. *Nat Protoc* 4:1350-1362.
 58. Benjamin, C. L., V. O. Melnikova, and H. N. Ananthaswamy. 2008. P53 protein and pathogenesis of melanoma and nonmelanoma skin cancer. *Adv Exp Med Biol* 624:265-282.
 59. Oro, A. E., K. M. Higgins, Z. Hu, J. M. Bonifas, E. H. Epstein, Jr., and M. P. Scott. 1997. Basal cell carcinomas in mice overexpressing sonic hedgehog. *Science* 276:817-821.
 60. Waikel, R. L., Y. Kawachi, P. A. Waikel, X. J. Wang, and D. R. Roop. 2001. Deregulated expression of c-Myc depletes epidermal stem cells. *Nat Genet* 28:165-168.

61. Langton, A. K., S. E. Herrick, and D. J. Headon. 2008. An extended epidermal response heals cutaneous wounds in the absence of a hair follicle stem cell contribution. *J Invest Dermatol* 128:1311-1318.
62. Coulombe, P. A. 1997. Towards a molecular definition of keratinocyte activation after acute injury to stratified epithelia. *Biochem Biophys Res Commun* 236:231-238.
63. Herber, R., A. Liem, H. Pitot, and P. F. Lambert. 1996. Squamous epithelial hyperplasia and carcinoma in mice transgenic for the human papillomavirus type 16 E7 oncogene. *J Virol* 70:1873-1881.
64. Song, S., H. C. Pitot, and P. F. Lambert. 1999. The human papillomavirus type 16 E6 gene alone is sufficient to induce carcinomas in transgenic animals. *J Virol* 73:5887-5893.
65. Rodewald, H. R., S. Paul, C. Haller, H. Bluethmann, and C. Blum. 2001. Thymus medulla consisting of epithelial islets each derived from a single progenitor. *Nature* 414:763-768.
66. Bleul, C. C., T. Corbeaux, A. Reuter, P. Fisch, J. S. Monting, and T. Boehm. 2006. Formation of a functional thymus initiated by a postnatal epithelial progenitor cell. *Nature* 441:992-996.
67. Rounbehler, R. J., R. Schneider-Broussard, C. J. Conti, and D. G. Johnson. 2001. Myc lacks E2F1's ability to suppress skin carcinogenesis. *Oncogene* 20:5341-5349.

68. Morris, R. J., S. M. Fischer, and T. J. Slaga. 1986. Evidence that a slowly cycling subpopulation of adult murine epidermal cells retains carcinogen. *Cancer Res* 46:3061-3066.
69. Watt, F. M., and K. B. Jensen. 2009. Epidermal stem cell diversity and quiescence. *EMBO Mol Med* 1:260-267.
70. Loh, Y. H., Q. Wu, J. L. Chew, V. B. Vega, W. Zhang, X. Chen, G. Bourque, J. George, B. Leong, J. Liu, K. Y. Wong, K. W. Sung, C. W. Lee, X. D. Zhao, K. P. Chiu, L. Lipovich, V. A. Kuznetsov, P. Robson, L. W. Stanton, C. L. Wei, Y. Ruan, B. Lim, and H. H. Ng. 2006. The Oct4 and Nanog transcription network regulates pluripotency in mouse embryonic stem cells. *Nat Genet* 38:431-440.
71. Sharov, A. A., S. Masui, L. V. Sharova, Y. Piao, K. Aiba, R. Matoba, L. Xin, H. Niwa, and M. S. Ko. 2008. Identification of Pou5f1, Sox2, and Nanog downstream target genes with statistical confidence by applying a novel algorithm to time course microarray and genome-wide chromatin immunoprecipitation data. *BMC Genomics* 9:269.
72. Orkin, S. H., J. Wang, J. Kim, J. Chu, S. Rao, T. W. Theunissen, X. Shen, and D. N. Levasseur. 2008. The transcriptional network controlling pluripotency in ES cells. *Cold Spring Harb Symp Quant Biol* 73:195-202.
73. Chen, L., A. Yabuuchi, S. Eminli, A. Takeuchi, C. W. Lu, K. Hochedlinger, and G. Q. Daley. 2009. Cross-regulation of the Nanog and Cdx2 promoters. *Cell Res* 19:1052-1061.
74. Young, M. R., J. J. Li, M. Rincon, R. A. Flavell, B. K. Sathyanarayana, R. Hunziker, and N. Colburn. 1999. Transgenic mice demonstrate AP-1 (activator

- protein-1) transactivation is required for tumor promotion. *Proc Natl Acad Sci U S A* 96:9827-9832.
75. Kangsamaksin, T., and R. J. Morris. 2011. Bone morphogenetic protein 5 regulates the number of keratinocyte stem cells from the skin of mice. *J Invest Dermatol* 131:580-585.
 76. Suzuki, A., A. Raya, Y. Kawakami, M. Morita, T. Matsui, K. Nakashima, F. H. Gage, C. Rodriguez-Esteban, and J. C. Izpisua Belmonte. 2006. Nanog binds to Smad1 and blocks bone morphogenetic protein-induced differentiation of embryonic stem cells. *Proc Natl Acad Sci U S A* 103:10294-10299.
 77. Tay, Y., J. Zhang, A. M. Thomson, B. Lim, and I. Rigoutsos. 2008. MicroRNAs to Nanog, Oct4 and Sox2 coding regions modulate embryonic stem cell differentiation. *Nature* 455:1124-1128.
 78. Guo, H., N. T. Ingolia, J. S. Weissman, and D. P. Bartel. 2010. Mammalian microRNAs predominantly act to decrease target mRNA levels. *Nature* 466:835-840.
 79. Bartel, D. P. 2004. MicroRNAs: genomics, biogenesis, mechanism, and function. *Cell* 116:281-297.
 80. Thomson, J. M., M. Newman, J. S. Parker, E. M. Morin-Kensicki, T. Wright, and S. M. Hammond. 2006. Extensive post-transcriptional regulation of microRNAs and its implications for cancer. *Genes Dev* 20:2202-2207.
 81. Johnson, S. M., H. Grosshans, J. Shingara, M. Byrom, R. Jarvis, A. Cheng, E. Labourier, K. L. Reinert, D. Brown, and F. J. Slack. 2005. RAS is regulated by the let-7 microRNA family. *Cell* 120:635-647.

82. Lee, Y. S., and A. Dutta. 2007. The tumor suppressor microRNA let-7 represses the HMGA2 oncogene. *Genes Dev* 21:1025-1030.
83. Tsang, W. P., and T. T. Kwok. 2008. Let-7a microRNA suppresses therapeutics-induced cancer cell death by targeting caspase-3. *Apoptosis* 13:1215-1222.
84. Takamizawa, J., H. Konishi, K. Yanagisawa, S. Tomida, H. Osada, H. Endoh, T. Harano, Y. Yatabe, M. Nagino, Y. Nimura, T. Mitsudomi, and T. Takahashi. 2004. Reduced expression of the let-7 microRNAs in human lung cancers in association with shortened postoperative survival. *Cancer Res* 64:3753-3756.
85. Heo, I., C. Joo, J. Cho, M. Ha, J. Han, and V. N. Kim. 2008. Lin28 mediates the terminal uridylation of let-7 precursor MicroRNA. *Mol Cell* 32:276-284.
86. Heo, I., C. Joo, Y. K. Kim, M. Ha, M. J. Yoon, J. Cho, K. H. Yeom, J. Han, and V. N. Kim. 2009. TUT4 in concert with Lin28 suppresses microRNA biogenesis through pre-microRNA uridylation. *Cell* 138:696-708.
87. Liedtke, S., J. Enczmann, S. Waclawczyk, P. Wernet, and G. Kogler. 2007. Oct4 and its pseudogenes confuse stem cell research. *Cell Stem Cell* 1:364-366.
88. Poliseno, L., L. Salmena, J. Zhang, B. Carver, W. J. Haveman, and P. P. Pandolfi. 2010. A coding-independent function of gene and pseudogene mRNAs regulates tumour biology. *Nature* 465:1033-1038.
89. Smirnova, L., A. Grafe, A. Seiler, S. Schumacher, R. Nitsch, and F. G. Wulczyn. 2005. Regulation of miRNA expression during neural cell specification. *Eur J Neurosci* 21:1469-1477.

90. Rybak, A., H. Fuchs, L. Smirnova, C. Brandt, E. E. Pohl, R. Nitsch, and F. G. Wulczyn. 2008. A feedback loop comprising lin-28 and let-7 controls pre-let-7 maturation during neural stem-cell commitment. *Nat Cell Biol* 10:987-993.
91. Zhang, Y., T. Chao, R. Li, W. Liu, Y. Chen, X. Yan, Y. Gong, B. Yin, B. Qiang, J. Zhao, J. Yuan, and X. Peng. 2009. MicroRNA-128 inhibits glioma cells proliferation by targeting transcription factor E2F3a. *J Mol Med* 87:43-51.
92. Godlewski, J., M. O. Nowicki, A. Bronisz, S. Williams, A. Otsuki, G. Nuovo, A. Raychaudhury, H. B. Newton, E. A. Chiocca, and S. Lawler. 2008. Targeting of the Bmi-1 oncogene/stem cell renewal factor by microRNA-128 inhibits glioma proliferation and self-renewal. *Cancer Res* 68:9125-9130.
93. Khan, A. P., L. M. Poisson, V. B. Bhat, D. Fermin, R. Zhao, S. Kalyana-Sundaram, G. Michailidis, A. I. Nesvizhskii, G. S. Omenn, A. M. Chinnaiyan, and A. Sreekumar. 2010. Quantitative proteomic profiling of prostate cancer reveals a role for miR-128 in prostate cancer. *Mol Cell Proteomics* 9:298-312.
94. Ambs, S., R. L. Prueitt, M. Yi, R. S. Hudson, T. M. Howe, F. Petrocca, T. A. Wallace, C. G. Liu, S. Volinia, G. A. Calin, H. G. Yfantis, R. M. Stephens, and C. M. Croce. 2008. Genomic profiling of microRNA and messenger RNA reveals deregulated microRNA expression in prostate cancer. *Cancer Res* 68:6162-6170.
95. Simon, J. A., and R. E. Kingston. 2009. Mechanisms of polycomb gene silencing: knowns and unknowns. *Nat Rev Mol Cell Biol* 10:697-708.

96. Lukacs, R. U., S. Memarzadeh, H. Wu, and O. N. Witte. 2010. Bmi-1 is a crucial regulator of prostate stem cell self-renewal and malignant transformation. *Cell Stem Cell* 7:682-693.
97. Kim, J., A. J. Woo, J. Chu, J. W. Snow, Y. Fujiwara, C. G. Kim, A. B. Cantor, and S. H. Orkin. 2010. A Myc network accounts for similarities between embryonic stem and cancer cell transcription programs. *Cell* 143:313-324.
98. Salmena, L., L. Poliseno, Y. Tay, L. Kats, and P. P. Pandolfi. 2011. A ceRNA hypothesis: the Rosetta Stone of a hidden RNA language? *Cell* 146:353-358.
99. Choi, Y. J., C. P. Lin, J. J. Ho, X. He, N. Okada, P. Bu, Y. Zhong, S. Y. Kim, M. J. Bennett, C. Chen, A. Ozturk, G. G. Hicks, G. J. Hannon, and L. He. 2011. miR-34 miRNAs provide a barrier for somatic cell reprogramming. *Nat Cell Biol* 13:1353-1360.

Vita

Mark Daniel Badeaux was born in Monroe Louisiana in 1977 to two loving parents, Gilbert Ray Badeaux and Kathleen Scott Badeaux. He spent his formative years searching for Voltron lions, and attended school as a diversion from this activity. After graduating from Highland High School in Gilbert, AZ, he attended the University of Arizona in Tucson, where he majored in indecisiveness, Atmospheric Science, and English Literature. Giving all of these subjects a miss, he transferred to the University of Texas at Austin, where he graduated with a Bachelors of Science in Microbiology in 2002. Attempting to integrate himself into the “real world,” he worked in a bacteriology lab at the Texas Dept. of State Health Services (DSHS), then as a quality assurance scientist at Abbott Labs, and finally in the foodborne epidemiology unit of DSHS. His innate curiosity and desire to make a meaningful contribution to cancer research led him to the University of Texas at Houston GSBS and MD Anderson Cancer Center in the Fall of 2005. To be continued...